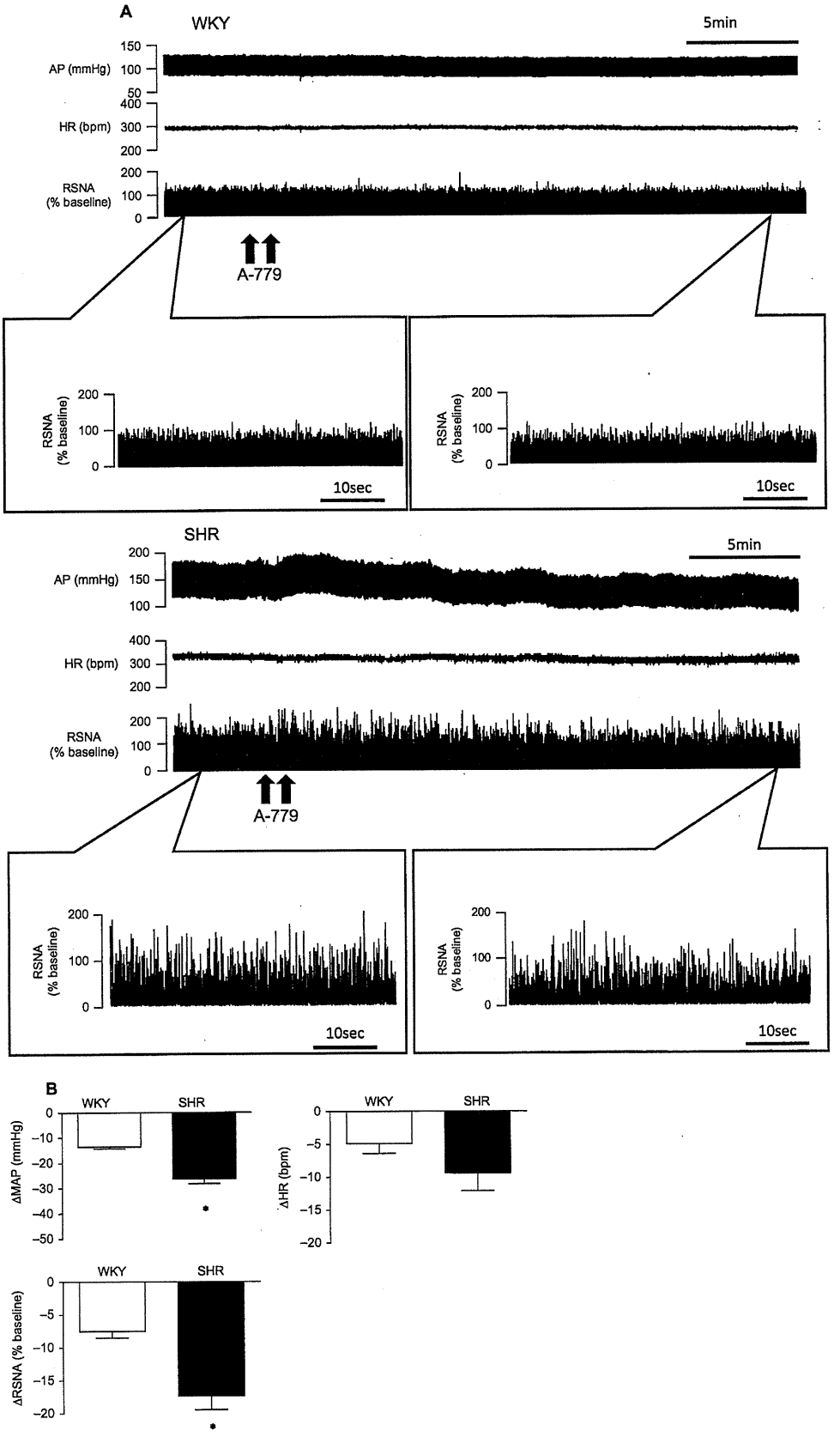

Figure 2. Effect of bilateral microinjection of A-779 on AP, HR, and renal sympathetic nerve activity (RSNA). **A,** Original recording form WKY (top) and SHR (bottom) rats showing AP, HR, and RSNA in response to bilateral microinjection of A-779 (100 pmol) into the RVLM. Arrows indicate the time at which A-779 was injected. **B,** Grouped data of mean (+ SEM) change from baseline of MAP, HR, and RSNA evoked by bilateral microinjection of A-779 into the RVLM. n = 5 per group. *P < 0.05 compared to WKY rats.

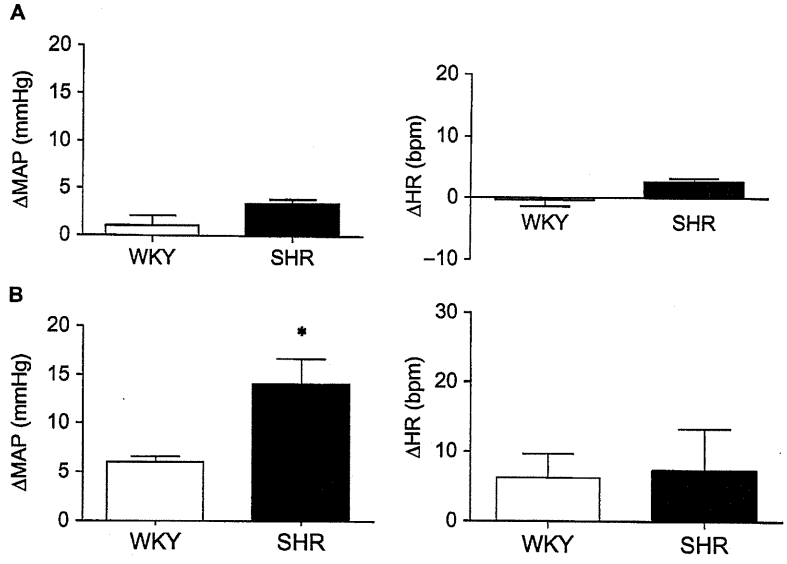

Figure 3. The effect of the microinjection of Ang-(1-7) into the RVLM pretreated with angiotensin antagonists. **A,** Group data of the mean (+SEM) change in MAP and HR in response to microinjection of Ang-(1-7) (100 pmol) pretreated with A-779 (100 pmol). **B,** Group data of the mean (+SEM) change in MAP and HR in response to microinjection with Ang-(1-7) (100 pmol) pretreated valsartan (100 pmol). n = 5 per group. *P < 0.05 compared to WKY rats.

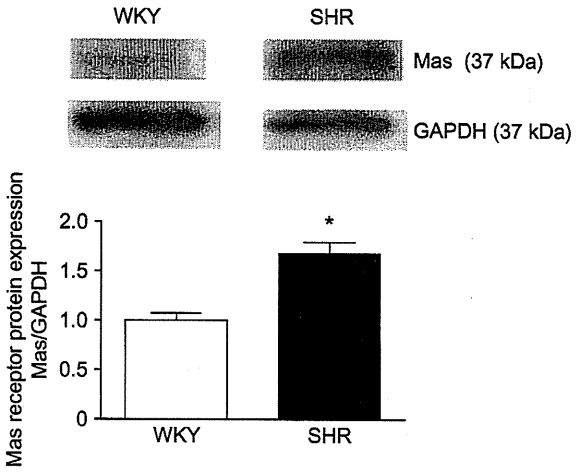

Figure 4. Western blot analysis demonstrating Mas receptor expression in the RVLM. Data are expressed as the ratio relative to GAPDH levels. n= 4 per group. *P < 0.05 compared to WKY rats.

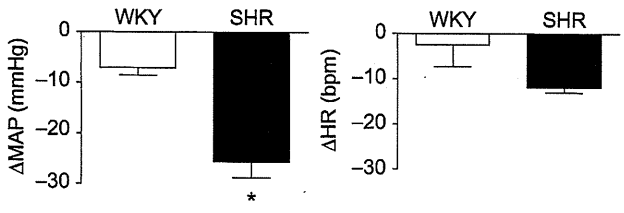

Figure 5. The effect of bilateral microinjection of ACE2 inhibitor DX600 on AP and HR. Grouped data of mean (+SEM) change in MAP and HR evoked by bilateral microinjection of DX600 (25 pmol) into the RVLM. n = 5 per group. *P < 0.05 compared with WKY rats.

significantly decreased AP and RSNA in both WKY and SHR, but the decrease was greater in SHR than in WKY; 2) microinjection of Ang-(1-7) into the RVLM increased AP, and this effect was blocked by the selective Ang-(1-7) antagonist A-779, but not by the AT_1 receptor blocker valsartan; and 3) Mas receptor expression levels in the RVLM were greater in SHRs than in WKYs. Together, these results suggest that endogenous Ang-(1-7) in the RVLM contributes to the maintenance of AP and its activity might be enhanced in SHR compared to WKY.

Our observations are consistent with previous reports that microinjection of Ang-(1-7) into the RVLM increases AP (18,22). Electrophysiological studies demonstrated that most neurons in the PVN are excited by Ang-(1-7) (23), and the Ang-(1-7)-induced firing rate increase of PVN neurons is blocked by A-779 (24). Paraventricular nucleus neurons have excitatory efferents to the RVLM (23, 24). Thus, endogenous Ang-(1-7) likely has a stimulatory effect on RVLM neurons.

Microinjection of AT_1 receptor antagonists into the RVLM decreases AP in SHR but not in control WKY (9,25), suggesting that AT_1 receptors in the RVLM are not activated under baseline conditions in normotensive rats, but AT_1 receptors in the RVLM are tonically stimulated and act to support sympathetic vasomotor tone under basal conditions in SHR. Microinjection of the Ang-(1-7) antagonist A-779 into the RVLM, however, decreased AP in both strains, and the hypotensive effect was greater in SHR than in WKY. These data suggest that the RVLM neurons are tonically stimulated by

endogenous Ang-(1-7) in normal conditions and their stimulation is augmented in SHR.

In the present study, the effect of Ang-(1-7) in the RVLM was not mediated by the AT_1 receptor, but was mediated by the Mas receptor. Previous studies also showed that Ang-(1-7) is an endogenous ligand of the orphan G-protein coupled receptor Mas (11). In fact, the binding of Ang-(1-7) in the kidney and the antidiuretic action of Ang-(1-7) are completely abolished in Mas-knockout mice (11) and Ang-(1-7) also does not induce relaxation in the aorta of Mas-knockout mice (11). These data indicate that Mas is a functional receptor that mediates the physiological actions of Ang-(1-7).

Ang-(1-7) acts as a counterregulatory modulator of Ang II in the central nervous system (4).While Ang II reduces the baroreflex sensitivity (26), Ang-(1-7) facilitates the baroreflex after either intracerebroventricular infusion (27,28) or microinjection into the NTS (29,30), but does not alter the baroreflex after microinjection into the RVLM (31). In the present study, we did not investigate the effect of Ang-(1-7) on baroreflex sensitivity.

The observations that exogenous stimulation of Mas receptors elicits a greater increase in AP and blockade of Mas receptors induces a greater decrease in AP in SHR might relate to an increase in the number of receptors in the RVLM of SHR. Mas receptor protein expression in the RVLM was significantly higher in SHR than in WKY. These findings suggest that activation of the Ang-(1-7)-Mas pathway in the RVLM contributes to the maintenance and increase in AP in SHR.

Recently, ACE2 was identified as a new member of the ACE family (32). This carboxypeptidase cleaves Ang I and Ang II to form Ang-(1-9) and Ang-(1-7), respectively (10,33). ACE2 has an approximately 400-fold greater affinity for Ang II than for Ang I (33). Accordingly, the major role of ACE2 in angiotensin peptide metabolism is the production of Ang-(1-7). In the present study, microinjection of the ACE2 inhibitor DX600 into the RVLM induced a significant decrease in AP in both SHR and WKY, although the decrease in AP was significantly greater in SHR than in WKY. Therefore, we suggest that DX600 into the RVLM might also decrease RSNA as A-779, although we did not measure RSNA directly in the case of DX600. Microinjection of either Ang II or Ang-(1-7) into the RVLM or NTS increases or decreases AP, respectively (18,29). Injection of the ACE2 inhibitor MLN4760 into the NTS decreases AP in normotensive Sprague Dawley rats (34), and in the present study, microinjection of the ACE2 inhibitor DX600 into the RVLM induced a decrease in AP. Injecting an ACE2 inhibitor into the RVLM should decrease Ang-(1-7) levels, providing a potential mechanism for the AP response, although Ang II levels may also increase.

Ang-(1-7) is also formed by the endopeptidase neprilysin from Ang-I or Ang-(1–9) (35). Neprilysin mRNA in the medulla is lower in older rats compared to younger rats, whereas ACE2 and Mas receptor mRNA levels of older rats do not differ from those in younger rats (36). Thus, functional studies are necessary to confirm the altered expression or activity of neprilysin in WKY and SHR. ACE2 might also be involved in the metabolism of other peptides that are not related to RAS, such as apelin, neurotensin, and dynorphin (33,37). Microinjection of neurotensin and apelin into the RVLM increase AP (38,39). Apelin expression is enhanced in the RVLM in SHR compared to WKY (40); thus it is possible that the effect of apelin in the RVLM is also altered in SHR.

Although Ang-(1-7) is reported to play an important role in counteracting the pressor and proliferative actions of Ang II in the heart or vasculature (41,42), in the present study Ang-(1-7) had effects that were similar to those of Ang II in the RVLM. It is not clear why the systemic and central effects of Ang-(1-7) and Ang II are different; Ang-(1-7) may have a distinct mechanism of action in neuronal nuclei such as the RVLM. In addition, the precise mechanism(s) involved in the differences in BP regulation induced by endogenous Ang-(1-7) in the RVLM between SHR and WKY is uncertain because we did not measure endogenous Ang-(1-7) activity directly or Ang-(1-7) concentration in the RVLM.

In conclusion, the findings from the present study suggest that endogenous Ang-(1-7) in the RVLM contributes to tonic maintenance of AP via the sympathetic nervous system both in WKY and SHR and that its activity in Ang-(1-7)-Mas receptor axis might be enhanced in SHR.

ACKNOWLEDGMENTS

This study was supported by a grant-in-aid for scientific research from the Japan Society for the Promotion of Science (B19390231), and in part, by a Health and Labor Sciences Research Grant of Japan. We express our sincere thanks to Naomi Shiouze for help with the western blot analysis.

Declaration of interest: The authors report no conflicts of interest. The authors alone are responsible for the content and writing of the paper.

REFERENCES

[1] Grassi G. Assessment of sympathetic cardiovascular drive in human hypertension: Achievements and perspectives. *Hypertension* 2009;54:690–697.

[2] Esler M. The 2009 Carl Ludwig Lecture: Pathophysiology of the human sympathetic nervous system in cardiovascular diseases: The transition from mechanisms to medical management. *J Appl Physiol* 2010;108:227–237.

[3] Guyenet PG. The sympathetic control of blood pressure. *Nat Rev Neurosci* 2006;7:335–346.
[4] Xia H, Lazartigues E. Angiotensin-converting enzyme 2 in the brain: Properties and future directions. *J Neurochem* 2008;107:1482–1494.
[5] Veerasingham SJ, Raizada MK. Brain renin-angiotensin system dysfunction in hypertension: Recent advances and perspectives. *Br J Pharmacol* 2003;139:191–202.
[6] Kishi T, Hirooka Y, Kimura Y, Ito K, Shimokawa H, Takeshita A. Increased reactive oxygen species in rostral ventrolateral medulla contribute to neural mechanisms of hypertension in stroke-prone spontaneously hypertensive rats. *Circulation* 2004;109:2357–2362.
[7] Fontes MA, Martins Pinge MC, Naves V, Campagnole-Santos MJ, Lopes OU, Khosla MC, Santos RA. Cardiovascular effects produced by microinjection of angiotensins and angiotensin antagonists into the ventrolateral medulla of freely moving rats. *Brain Res* 1997;750:305–310.
[8] Tagawa T, Fontes MA, Potts PD, Allen AM, Dampney RA. The physiological role of AT1 receptors in the ventrolateral medulla. *Braz J Med Biol Res* 2000;33:643–652.
[9] Ito S, Komatsu K, Tsukamoto K, Kanmatsuse K, Sved AF. Ventrolateral medulla AT_1 receptors support blood pressure in hypertensive rats. *Hypertension* 2002;40:552–559.
[10] Tipnis SR, Hooper NM, Hyde R, Karran E, Christie G, Turner AJ. A human homolog of angiotensin-converting enzyme. cloning and functional expression as a captopril-insensitive carboxypeptidase. *J Biol Chem* 2000;275:33238–33243.
[11] Santos RA, Simoes e Silva AC, Maric C, Silva DM, Machado RP, de Buhr I, Heringer-Walther S, Pinheiro SV, Lopes MT, Bader M, Mendes EP, Lemos VS, Campagnole-Santos MJ, Schultheiss HP, Speth R, Walther T. Angiotensin-(1-7) is an endogenous ligand for the G protein-coupled receptor mas. *Proc Natl Acad Sci U S A* 2003;100:8258–8263.
[12] Campagnole-Santos MJ, Diz DI, Santos RA, Khosla MC, Brosnihan KB, Ferrario CM. Cardiovascular effects of angiotensin-(1-7) injected into the dorsal medulla of rats. *Am J Physiol* 1989; 257:H324–H329.
[13] Silva LC, Fontes MA, Campagnole-Santos MJ, Khosla MC, Campos RR Jr, Guertzenstein PG, Santos RA. Cardiovascular effects produced by micro-injection of angiotensin-(1-7) on vasopressor and vasodepressor sites of the ventrolateral medulla. *Brain Res* 1993;613:321–325.
[14] Fontes MA, Baltatu O, Caligiorne SM, Campagnole-Santos MJ, Ganten D, Bader M, Santos RA. Angiotensin peptides acting at rostral ventrolateral medulla contribute to hypertension of TGR(mREN2)27 rats. *Physiol Genomics* 2000;2: 137–142.
[15] Silva AQ, Santos RA, Fontes MA. Blockade of endogenous angiotensin-(1-7) in the hypothalamic paraventricular nucleus reduces renal sympathetic tone. *Hypertension* 2005;46: 341–348.
[16] Doobay MF, Talman LS, Obr TD, Tian X, Davisson RL, Lazartigues E. Differential expression of neuronal ACE2 in transgenic mice with overexpression of the brain renin-angiotensin system. *Am J Physiol Regul Integr Comp Physiol* 2007;292:R373–R381.
[17] Becker LK, Etelvino GM, Walther T, Santos RA, Campagnole-Santos MJ. Immunofluorescence localization of the receptor mas in cardiovascular-related areas of the rat brain. *Am J Physiol Heart Circ Physiol* 2007;293:H1416–H1424.
[18] Fontes MA, Silva LC, Campagnole-Santos MJ, Khosla MC, Guertzenstein PG, Santos RA. Evidence that angiotensin-(1-7) plays a role in the central control of blood pressure at the ventro-lateral medulla acting through specific receptors. *Brain Res* 1994;665:175–180.
[19] Zhou LM, Shi Z, Gao J, Han Y, Yuan N, Gao XY, Zhu GQ. Angiotensin-(1-7) and angiotension II in the rostral ventrolateral medulla modulate the cardiac sympathetic afferent reflex and sympathetic activity in rats. *Pflugers Arch* 2010;459: 681–688.
[20] Ito K, Hirooka Y, Sakai K, Kishi T, Kaibuchi K, Shimokawa H, Takeshita A. Rho/Rho-kinase pathway in brain stem contributes to blood pressure regulation via sympathetic nervous system: Possible involvement in neural mechanisms of hypertension. *Circ Res* 2003;92:1337–1343.
[21] Koga Y, Hirooka Y, Araki S, Nozoe M, Kishi T, Sunagawa K. High salt intake enhances blood pressure increase during development of hypertension via oxidative stress in rostral ventrolateral medulla of spontaneously hypertensive rats. *Hypertens Res* 2008;31:2075–2083.
[22] Santos RA, Campagnole-Santos MJ, Baracho NCV, Fontes MAP, Silva LCS, Neves LAA, Oliveira DR, Caligiorne SM, Rodrigues AR, Gropen C Jr, Carvalho WS, Simoes e Silva AC, Khosla MC. Characterization of a new angiotensin antagonist selective for angiotensin-(1-7): Evidence that the actions of angiotensin-(1-7) are mediated by specific angiotensin receptors. *Brain Res Bull* 1994;35:293–298.
[23] Felix D, Khosla MC, Barnes KL, Imboden H, Montani B, Ferrario CM. Neurophysiological responses to angiotensin-(1-7). *Hypertension* 1991;17:1111–1114.
[24] Ambuhl P, Felix D, Khosla MC. 7-D-ALA]-angiotensin-(1-7): Selective antagonism of angiotensin-(1-7) in the rat paraventricular nucleus. *Brain Res Bull* 1994;35:289–291.
[25] Potts PD, Allen AM, Horiuchi J, Dampney RA. Does angiotensin II have a significant tonic action on cardiovascular neurons in the rostral and caudal VLM? *Am J Physiol Regul Integr Comp Physiol* 2000;279:R1392–R1402.
[26] Casto R, Phillips MI. Angiotensin II attenuates baroreflexes at nucleus tractus solitarius of rats. *Am J Physiol* 1986;250: R193–R198.
[27] Britto RR, Santos RA, Fagundes-Moura CR, Khosla MC, Campagnole-Santos MJ. Role of angiotensin-(1-7) in the modulation of the baroreflex in renovascular hypertensive rats. *Hypertension* 1997;30:549–556.
[28] Oliveira DR, Santos RA, Santos GF, Khosla M, Campagnole-Santos MJ. Changes in the baroreflex control of heart rate produced by central infusion of selective angiotensin antagonists in hypertensive rats. *Hypertension* 1996;27:1284–1290.
[29] Chaves GZ, Caligiorne SM, Santos RA, Khosla MC, Campagnole-Santos MJ. Modulation of the baroreflex control of heart rate by angiotensin-(1-7) at the nucleus tractus solitarii of normotensive and spontaneously hypertensive rats. *J Hypertens* 2000;18:1841–1848.
[30] Couto AS, Baltatu O, Santos RA, Ganten D, Bader M, Campagnole-Santos MJ. Differential effects of angiotensin II and angiotensin-(1-7) at the nucleus tractus solitarii of transgenic rats with low brain angiotensinogen. *J Hypertens* 2002;20:919–925.
[31] Alzamora AC, Santos RA, Campagnole-Santos MJ. Baroreflex modulation by angiotensins at the rat rostral and caudal ventrolateral medulla. *Am J Physiol Regul Integr Comp Physiol* 2006;290:R1027–R1034.
[32] Donoghue M, Hsieh F, Baronas E, Godbout K, Gosselin M, Stagliano N, Donovan M, Woolf B, Robison K, Jeyaseelan R, Breitbart RE, Acton S. A novel angiotensin-converting enzyme-related carboxypeptidase (ACE2) converts angiotensin I to angiotensin 1-9. *Circ Res* 2000;87:E1–E9.
[33] Vickers C, Hales P, Kaushik V, Dick L, Gavin J, Tang J, Godbout K, Parsons T, Baronas E, Hsieh F, Acton S, Patane M, Nichols A, Tummino P. Hydrolysis of biological peptides by human angiotensin-converting enzyme-related carboxypeptidase. *J Biol Chem* 2002;277:14838–14843.
[34] Diz DI, Garcia-Espinosa MA, Gegick S, Tommasi EN, Ferrario CM, Ann Tallant E, Chappell MC, Gallagher PE. Injections of angiotensin-converting enzyme 2 inhibitor MLN4760 into nucleus tractus solitarii reduce baroreceptor reflex sensitivity for heart rate control in rats. *Exp Physiol* 2008;93:694–700.

[35] Rice GI, Thomas DA, Grant PJ, Turner AJ, Hooper NM. Evaluation of angiotensin-converting enzyme (ACE), its homologue ACE2 and neprilysin in angiotensin peptide metabolism. *Biochem J* 2004;383:45–51.

[36] Sakima A, Averill DB, Gallagher PE, Kasper SO, Tommasi EN, Ferrario CM, Diz DI. Impaired heart rate baroreflex in older rats: Role of endogenous angiotensin-(1-7) at the nucleus tractus solitarii. *Hypertension* 2005;46:333–340.

[37] Warner FJ, Smith AI, Hooper NM, Turner AJ. Angiotensin-converting enzyme-2: A molecular and cellular perspective. *Cell Mol Life Sci* 2004;61:2704–2713.

[38] Ishizuka T, Wei X, Kubo T. Cardiovascular effects of microinjections of thyrotropin-releasing hormone, oxytocin and other neuropeptides into the rostral ventrolateral medulla of the rat. *Arch Int Pharmacodyn Ther* 1993;322:35–44.

[39] Seyedabadi M, Goodchild AK, Pilowsky PM. Site-specific effects of apelin-13 in the rat medulla oblongata on arterial pressure and respiration. *Auton Neurosci* 2002;101:32–38.

[40] Zhang Q, Yao F, Raizada MK, O'Rourke ST, Sun C. Apelin gene transfer into the rostral ventrolateral medulla induces chronic blood pressure elevation in normotensive rats. *Circ Res* 2009;104:1421–1428.

[41] Averill DB, Ishiyama Y, Chappell MC, Ferrario CM. Cardiac angiotensin-(1-7) in ischemic cardiomyopathy. *Circulation* 2003;108:2141–2146.

[42] Xu P, Costa-Goncalves AC, Todiras M, Rabelo LA, Sampaio WO, Moura MM, Santos SS, Luft FC, Bader M, Gross V, Alenina N, Santos RA. Endothelial dysfunction and elevated blood pressure in MAS gene-deleted mice. *Hypertension* 2008;51:574–580.

EUROPEAN SOCIETY OF CARDIOLOGY®

Cardiovascular Research
doi:10.1093/cvr/cvr108

Inhibition of MDM2 attenuates neointimal hyperplasia via suppression of vascular proliferation and inflammation

Toru Hashimoto[1], Toshihiro Ichiki[1,2]*, Jiro Ikeda[1], Eriko Narabayashi[1], Hirohide Matsuura[1], Ryohei Miyazaki[1], Keita Inanaga, Kotaro Takeda[1,2], and Kenji Sunagawa[1]

[1]Department of Cardiovascular Medicine, Kyushu University Graduate School of Medical Sciences, Fukuoka, Japan; and [2]Department of Advanced Therapeutics for Cardiovascular Diseases, Kyushu University Graduate School of Medical Sciences, Fukuoka, Japan

Received 26 August 2010; revised 16 March 2011; accepted 8 April 2011

Time for primary review: 43 days

Aims Tumour protein p53 plays an important role in the vascular remodelling process as well as in oncogenesis. p53 is negatively regulated by murine double minute 2 (MDM2). A recently developed MDM2 inhibitor, nutlin-3, is a non-genotoxic activator of the p53 pathway. So far, the effect of MDM2 inhibition on vascular remodelling has not been elucidated. We therefore investigated the effect of nutlin-3 on neointima formation.

Methods and results Nutlin-3 up-regulated p53 and its downstream target p21 in vascular smooth muscle cells (VSMCs). DNA synthesis assay and flow cytometric analysis revealed that nutlin-3 inhibited platelet-derived growth factor (PDGF)-induced VSMC proliferation by cell cycle arrest. This inhibitory effect was abrogated in p53-siRNA-transfected VSMCs. Furthermore, nutlin-3 inhibited PDGF-stimulated VSMC migration. Treatment with nutlin-3 attenuated neointimal hyperplasia at 28 days after vascular injury in mice, associated with up-regulation of p53 and p21. BrdU incorporation was decreased at 14 days after injury in nutlin-3-treated mice. TUNEL assay showed that nutlin-3 did not exaggerate apoptosis of the injured vessels. Infiltration of macrophages and T-lymphocytes and mRNA expression of chemokine (C-C motif) ligand-5, interleukin-6, and intercellular adhesion molecule-1 were decreased in the injured vessels of nutlin-3-treated mice. Nutlin-3 suppressed NF-κB activation in VSMCs, but not in p53-siRNA-transfected VSMCs.

Conclusions The MDM2 antagonist nutlin-3 inhibits VSMC proliferation, migration, and NF-κB activation, and also attenuates neointimal hyperplasia after vascular injury in mice, which is associated with suppression of vascular cell proliferation and an inflammatory response. Targeting MDM2 might be a potential therapeutic strategy for the treatment of vascular proliferative diseases.

Keywords MDM2 • p53 • Proliferation • Inflammation • Neointima

1. Introduction

Vascular proliferation and inflammation, in which vascular smooth muscle cells (VSMCs) are involved profoundly, contribute to the pathophysiology of cardiovascular diseases including atherosclerosis, post-intervention restenosis, vein bypass graft failure, and transplant vasculopathy. Although the drug-eluting stent technology has reduced restenosis after coronary intervention, further elucidation of molecular mechanisms of vascular inflammation and proliferation is required for the retainment of vascular patency and reduction of cardiovascular events.[1–3]

The tumour protein p53 (Tp53) governs fundamental cellular processes such as apoptosis, cell cycle arrest, senescence, DNA repair, and cellular metabolism by regulating the transcription of many genes in response to stress signals.[4] p53 is believed to be involved in cardiovascular pathogenesis, however, the role of p53 in atherosclerotic diseases is Janus-faced. p53 deficiency exacerbates atherosclerosis in genetic dyslipidemic mice models,[5–8] while p53 overexpression enhances atherosclerotic plaque rupture.[9]

p53 expression is regulated by numerous proteins; more than 160 studies have been reported to date. Among them, murine double

* Corresponding author: Department of Cardiovascular Medicine, Kyushu University Graduate School of Medical Sciences, 3-1-1 Maidashi, Higashi-ku, 812-8582 Fukuoka, Japan. Tel: +81 92 642 5358; fax: +81 92 642 5374, Email: ichiki@cardiol.med.kyushu-u.ac.jp

minute 2 (MDM2) is regarded outstanding because it functions as a specific and indispensable inhibitor of p53 during embryonic development and its expression level is frequently affected in cancers.[10] MDM2 inhibits p53 transcriptional activity by occluding the transactivation domain to interrupt a recruitment of co-activators, and ubiquitinates the C-terminal domain of p53 to promote degradation by proteasome.[11]

MDM2 is overexpressed in human atherosclerotic tissues,[12] and in VSMCs of patients with primary aldosteronism,[13] indicating that MDM2 participates in pathological vascular remodelling. These studies also suggest that p53 might be suppressed by MDM2 in vascular proliferating process; therefore reactivation of the p53 pathway may be a novel therapeutic strategy for the treatment of vascular remodelling.

Disruption of the MDM2-p53 interaction has attracted an interest as a novel therapeutic strategy for cancers. Recently, a small-molecule inhibitor of MDM2-p53 binding, nutlin-3, was developed.[14] Nutlin-3 has antitumour effects by p53 activation in various cancer cells,[15] and *in vivo* administration induces tumour regression in mice.[14,16–19]

These studies prompted us to investigate the effects of nutlin-3 on vascular remodelling process, including VSMC proliferation and gene expression. In the present study, we showed that nutlin-3 inhibited platelet-derived growth factor (PDGF)-induced VSMC proliferation and NF-κB activation, and also attenuated neointimal hyperplasia after arterial injury in mice.

2. Methods

2.1 Materials

Dulbecco's modified Eagle's medium (DMEM) was purchased from Invitrogen (Carlsbad, CA, USA). Fetal bovine serum (FBS) was purchased from Nichirei Biosciences (Tokyo, Japan). Recombinant rat PDGF-BB was purchased from R&D Systems (Minneapolis, MN, USA). Bovine serum albumin (BSA), bromodeoxyuridine (BrdU), propidium iodide (PI), anti-α-tubulin antibody, and FITC-conjugated anti-α-smooth muscle actin antibody were from Sigma-Aldrich (St. Louis, MO, USA). Nutlin-3 was purchased from Cayman Chemical (Ann Arbor, MI, USA). Antibodies against p38MAPK, phospho-p38MAPK, ERK1/2, phospho-ERK1/2, JNK/SAPK, phospho-JNK/SAPK, p53, and histone H3 were purchased from Cell Signaling Technology (Beverly, MA, USA). Antibodies against p53, MDM2, PECAM-1, and Mac-3 were from Santa Cruz Biotechnology (Santa Cruz, CA, USA). Anti-p21 antibodies were from BD Biosciences Pharmingen (San Diego, CA, USA) and Imgenex (San Diego, CA, USA). Anti-CD3 antibody was from Abcam (Cambridge, MA, USA).

2.2 Cell cultures

VSMCs were isolated from the thoracic aorta of Sprague–Dawley rats (Kyudo Co., Saga, Japan). Cells were maintained in DMEM supplemented with 10% FBS at 37°C in a humidified atmosphere in 5% CO_2 in air. Before stimulation, cells were serum starved in DMEM with 0.1% BSA for 2 days.

2.3 Measurement of DNA synthesis

VSMCs pretreated with nutlin-3 (10 μmol/L) were stimulated with PDGF-BB (50 ng/mL) for 24 h and pulsed with [^{3}H]-thymidine (1 μCi/mL) for the last 6 h. Following washing with PBS, cells were incubated with 10% trichloroacetic acid, rinsed with a mixture of ethanol and diethylether (2:1), and dissolved in 0.5 N NaOH. The incorporation of [^{3}H]-thymidine into cells was measured by a liquid scintillation counter.

2.4 Flow cytometry

For cell cycle analysis, harvested VSMC were washed in PBS, and fixed in cold 70% ethanol. After treatment with RNase A (25 mg/mL) at 37°C for 60 min, cells were stained with PI (50 μg/mL) at 4°C for 30 min. Samples were analysed by BD FACSCalibur (Becton, Dickinson and Co., Franklin Lakes, NJ, USA). The cell cycle distribution was analysed by ModFit LT software (Verity Software House, Topsham, ME, USA). Apoptosis analysis was performed by using Annexin V-FITC Apoptosis Detection Kit I (BD Biosciences Pharmingen) and BD FACSCalibur according to the manufacturer's instructions.

2.5 Small-interfering RNA transfection

p53-targeting small-interfering RNA (siRNA) (#M-080060-00, a mixture of 4 siRNA: 5′ GAGAAUAUUUCACCCUUAA 3′; 5′ GCGACAGGGU CACCUAAUU 3′; 5′ GUACUCAAUUUCCCUCAAU 3′; 5′ CCACU AUCCACUACAAGUA 3′) and negative control non-targeting siRNA (D-001210-03) were purchased from Thermo Scientific Dharmacon (Lafayette, CO, USA). siRNA was introduced into VSMCs by a lipid transfection method. siRNA was mixed with lipofectamine RNAiMAX (Invitrogen, Carlsbad, CA, USA) in Opti-MEM I Reduced Serum Medium (Invitrogen) and incubated for 20 min at room temperature. VSMCs were transfected with the siRNA-lipofectamine complexes and incubated for 48 h at 37°C in a CO_2 incubator, and then used in the experiments.

2.6 Real-time reverse transcription polymerase chain reaction

Total RNA was extracted by the acid guanidinium thiocyanate–phenol chloroform extraction method. RNA was reverse transcribed using ReverTra Ace qPCR RT kit (TOYOBO, Osaka, Japan) according to the manufacturer's instructions. Real-time quantitative PCR (qPCR) was performed using THUNDERBIRD SYBR qPCR Mix (TOYOBO) and the Applied Biosystems 7500 real-time PCR system (Applied Biosystems, Foster City, CA, USA). Relative expression levels were determined by comparative Ct (ΔΔCt) method. *Hprt1* mRNA was used for standardization. Primer sequences used for amplification are as follows: <rat> *Tp53* (forward) 5′ GAGGTCGGCTCCGACTATACCA 3′, (reverse) 5′ AAAGCTGTCCCGTCCCAGAAG 3′; *Hprt1* (forward) 5′ TCCTCATG GACTGATTATGGACA 3′, (reverse) 5′ TAATCCAGCAGGTCAG CAAAGA 3′; <mouse> *Ccl5* (forward) 5′ ACCAGCAGCAAGTGC TCCAA 3′, (reverse) 5′ TGGCTAGGACTAGAGCAAGCAATG 3′; *Il6* (forward) 5′ CCACTTCACAAGTCGGAGGCTTA 3′, (reverse) 5′ GCAAGTGCATCATCGTTGTTCATAC 3′; *Icam1* (forward) 5′ GGCACCCAGCAGAAGTTGTT 3′, (reverse) 5′ CCTCAGTCACCTC TACCAAG 3′; *Hprt1* (forward) 5′ TTGTTGTTGGATATGCCCTT GACTA 3′, (reverse) 5′ AGGCAGATGGCCACAGGACTA 3′

2.7 Western blot analysis

Cells were harvested with lysis buffer composed of 1 × RIPA, 1% aprotinin, 10 μmol/L pepstatin A, 1 mmol/L PMSF, and 2.5 μg/mL leupepsin. Equal amounts of protein samples were subjected to SDS–PAGE and transferred to a polyvinylidene difluoride membrane (Immobilon-P, Millipore Corp., Billerica, MA, USA). After blocking with 5% skim milk, the membrane was incubated with a primary antibody, followed by a horseradish peroxidase (HRP)-conjugated secondary antibody. Blots were detected by chemiluminescence system using ECL Western Blotting Detection Reagent (GE Healthcare, Chalfont St Giles, UK). The membrane was exposed to X-ray film. The protein expression level was quantified by densitometry.

2.8 Cell migration assay (*in vitro* scratch assay)

VSMCs were plated onto the 35-mm dish coated with type I collagen and grown to be confluent. Following pretreatment with nutlin-3 (10 μmol/L) for 24 h, the VSMC monolayer was scraped with a pipet tip to create scratch wound, and then stimulated with PDGF-BB (50 ng/mL). After 24-h incubation, the number of cells which migrated into the scratch area was counted under microscopy.

2.9 DNA-binding ELISA for NF-κB

TransAM NF-κB p65 assay Kit (Active Motif, Carlsbad, CA, USA) was used. Equal amounts of nuclear extracts were added to the 96-well plate containing NF-κB consensus sequence and subjected to binding reaction for 1 h. Following incubation with anti-NF-κB p65 antibody for 1 h, samples were incubated with HRP-conjugated anti-IgG antibody for 1 h. Then samples were subjected to colorimetric reaction and absorbance at 450 nm was read by Mithras LB940 (Berthold Technologies, Bad Wildbad, Germany).

2.10 Animal experiments

All procedures were approved by the institutional animal use and care committee, and conducted in accordance with institutional guidelines and Guide for the Care and Use of Laboratory Animals (NIH Publication No. 85-23, revised 1996). C57B/6J male mice were purchased from CLEA Japan (Tokyo, Japan) and fed a normal chow. Mice (10-week-old) were anesthetized by intraperitoneal injection of 50 mg/kg pentobarbital, and then arterial wire injury was performed by insertion of a wire (0.38 mm in diameter. #C-SF-15-15, COOK, Bloomington, IN, USA) into the femoral artery as described previously.[20] Mini-osmotic pumps (Alzet, DURECT, Cupertino, CA, USA) delivering nutlin-3 (5 mg/kg/day) were placed into the intraperitonal space immediately after the vascular injury operation. BrdU (25 mg/kg) was injected at 24 and 1 h prior to tissue harvest. Mice were euthanized with injection of overdose pentobarbital. Harvested femoral arteries were fixed in 10% neutral-buffered formaldehyde solution. For RNA isolation, tissues were snap frozen in liquid nitrogen.

2.11 Morphometric analysis and immunohistochemistry

Neointimal and medial areas were quantified by NIH ImageJ software. Per cent stenosis was determined as the ratio of the intimal area and the area inside the internal elastic lamina × 100. For enzyme immunohistochemistry, paraffin-embedded tissue sections were deparaffinized and rehydrated, and then autoclaved in 10 mmol/L citrate buffer for antigen retrieval. Following quenching endogenous peroxidase and blocking with 3% skim milk, sections were incubated with primary antibodies at 4°C overnight. After incubation with biotinylated secondary antibodies and treatment with streptavidine-horseradish peroxidase conjugate, sections were incubated in 3,3′-diaminobenzidine solution and counterstained with haematoxylin. For fluorescent immunohistochemistry, sections were incubated with FITC-conjugated primary antibodies for 2 h at room temperature and then observed by fluorescent microscopy. Apoptotic cells were detected by the terminal deoxynucleotidyl transferase dUTP nick-end labelling (TUNEL) method with Apoptosis *in situ* Detection Kit (Wako Pure Chemical Industries, Osaka, Japan). Incorporated BrdU was detected using Cell Proliferation Kit (GE Healthcare UK).

2.12 Statistical analysis

Experimental data were analysed by one-way ANOVA and Fisher's *post hoc* test. Results are expressed as mean ± SEM. Values of $P < 0.05$ were considered statistically significant.

3. Results

3.1 Nutlin-3 activates p53 pathway and inhibits cellular proliferation and migration in VSMCs

At first, the effect of nutlin-3 on rat VSMC proliferation was examined. DNA synthesis assay showed that enhanced [^{3}H]-thymidine uptake induced by PDGF was dose dependently suppressed by nutlin-3 treatment in VSMCs (*Figure 1A*). We further assessed the effects of nutlin-3 on VSMC migration by *in vitro* scratch assay. Treatment with nutlin-3 attenuated VSMC migration induced by PDGF (*Figure 1B*).

We next verified whether nutlin-3 induces p53 in VSMCs. p53 protein expression was up-regulated by treatment with nutlin-3 (*Figure 1C*). p21 and MDM2, p53 downstream target molecules, were also up-regulated by nutlin-3 (*Figure 1C*), indicating functional activation of the p53 pathway in VSMCs. MAP kinases are known to be important mediators of PDGF signaling pathway.[21] However, nutlin-3 had no effects on the phosphorylation of p38MAPK, ERK1/2, and JNK/SAPK stimulated by PDGF (Supplementary material online, *Figure S1*). In order to exclude the possibility that the reduction of the number of proliferating cells was caused by apoptosis, we also evaluated VSMC apoptosis by flow cytometry. Treatment with nutlin-3 did not instigate apoptosis at basal condition and did not enhance H_2O_2-induced apoptosis either (*Figure 1D*). These results imply that the inhibitory effect of nutlin-3 on VSMC proliferation may not be attributable to inhibition of MAP kinases or induction of apoptosis.

3.2 Nutlin-3 induces cell cycle arrest in a p53-dependent manner in VSMCs

The effect of nutlin-3 on the cell cycle profile in rat VSMCs was analysed by flow cytometry. To confirm whether the inhibitory effect of nutlin-3 on cell proliferation depends on p53, assays were performed with or without p53 knock down by siRNA. Transfection of p53-targeting siRNA significantly down-regulated p53 mRNA expression in VSMCs, while transfection of control siRNA did not affect p53 mRNA expression levels (*Figure 2A*). Flow cytometric analysis revealed that the increase in the proportion of S-phase and the decrease in the proportion of G1-phase induced by PDGF was attenuated by treatment with nutlin-3 in VSMCs transfected with control siRNA (*Figure 2B*), whereas nutlin-3 failed to prevent cell cycle progression stimulated by PDGF in VSMCs transfected with p53-siRNA (*Figure 2B*). The cell cycle arrest-inducing effect of nutlin-3 was also abrogated in p53-deficient mouse VSMCs (Supplementary material online, *Figure S2*). These results suggest that nutlin-3 inhibited VSMC proliferation via p53-dependent cell cycle arrest at G1 phase.

3.3 Nutlin-3 attenuates neointimal hyperplasia after vascular injury

We next explored the effects of nutlin-3 on neointimal formation in mice. Administration of nutlin-3 (5 mg/kg/day) had no apparent effects on body weight and hemodynamics including blood pressure and heart rate (data not shown). No sickness behaviour and mortality occurred during the experimental period. No apparent macroscopic organ damage and tissue abnormalities were observed in nutlin-3-administered mice. Neointimal hyperplasia provoked by arterial wire-injury was significantly attenuated in nutlin-3-treated mice compared with control mice at 28 days after injury (*Figure 3A and B*). In both groups, most of the neointimal tissues were composed of α-smooth muscle actin (α-SMA) positive VSMCs (*Figure 3C*). Sirius red staining revealed that the neointimal tissues in both groups were also abundant in collagen fibres (*Figure 3D*). The collagen fibre hues under observation by polarizing microscopy were yellowish similarly

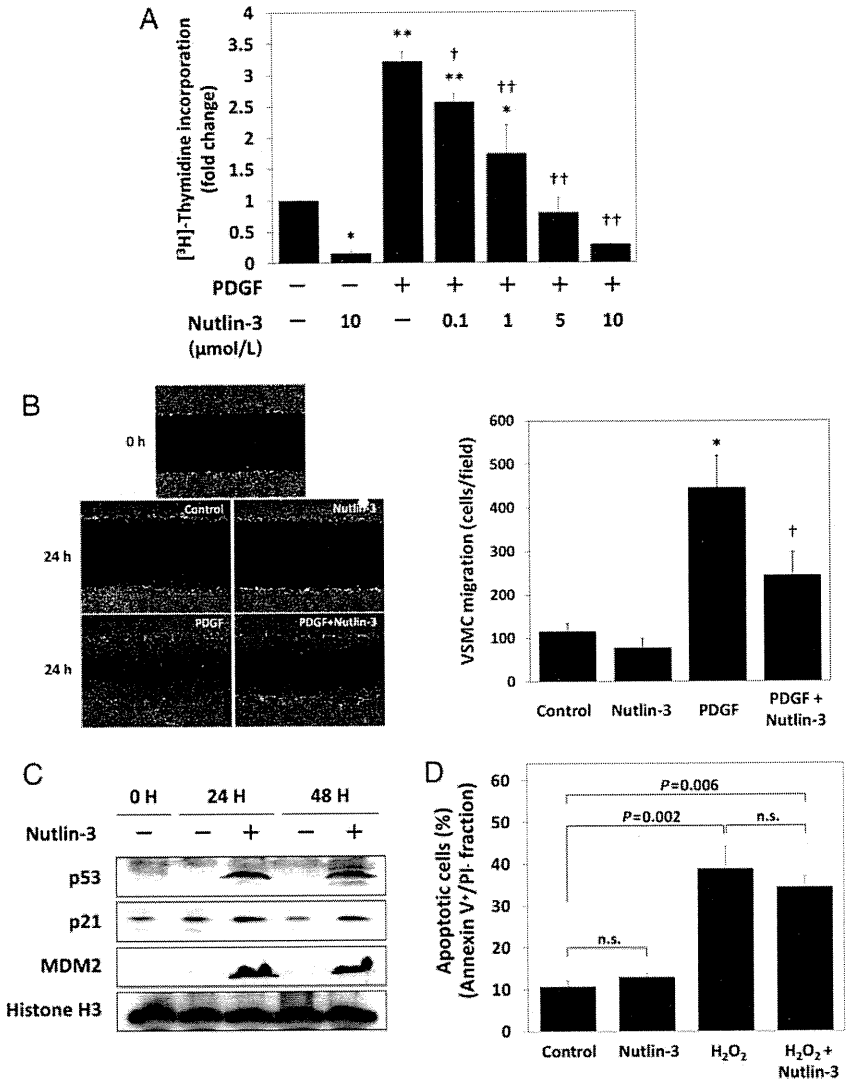

Figure 1 Effects of nutlin-3 on proliferation, migration, and p53 pathways in VSMCs. (*A*) VSMCs pretreated with nutlin-3 for 6 h were stimulated with PDGF-BB (50 ng/mL) for 24 h and [^{3}H]-thymidine incorporation was counted. $^*P < 0.05$, $^{**}P < 0.01$ vs. PDGF(−)-Nutlin-3(−); $^{\dagger}P < 0.05$, $^{\dagger\dagger}P < 0.01$ vs. PDGF(+)-Nutlin-3(−) ($n = 3$). (*B*) Effects of nutlin-3 on VSMC migration by *in vitro* scratch assay. VSMC monolayers were scratched and then stimulated with PDGF-BB (50 ng/mL) for 24 h in the presence or absence of nutlin-3. Nuclei were stained with DAPI. Representative micrographs and the quantitative analysis are shown. $^*P < 0.005$ vs. control, $^{\dagger}P < 0.05$ vs. PDGF ($n = 3$). (*C*) The expression levels of p53, p21, and MDM2 in VSMCs stimulated with nutlin-3 (10 μmol/L) were assessed by western blot analysis. Histone H3 was used for loading control. The same results were obtained in three other independent experiments. (*D*) The effect of nutlin-3 on VSMC apoptosis was analysed by flow cytometry. After pretreatment with nutlin-3 (10 μmol/L) for 24 h and incubation with H_2O_2 (5 mmol/L) for 1 h, VSMCs were stained with PI and Annexin V-FITC. The percentage of apoptotic cells (Annexin V-positive and PI-negative fraction) is shown. n.s.: not significant ($n = 3$). Values represent mean ± SEM.

in each group, suggesting that there would not be differences in collagen fibre properties affecting tissue stability (*Figure 3D*). Immunostaining of PECAM-1 showed that the luminal surface of the neointima was overlaid with endothelial cells in both control and nutlin-3 groups, indicating that administration of nutlin-3 did not impair re-endothelialization (*Figure 3E*). These results suggest that treatment with nutlin-3 attenuates neointimal overgrowth without affecting vascular tissue integrity. Expression of p53 and p21 was up-regulated in the vascular tissues of nutlin-3-administered mice compared with untreated mice (*Figure 3F*). MDM2 expression was unaffected by treatment with nutlin-3 (*Figure 3F*).

3.4 Effects of MDM2 inhibition on vascular proliferation and inflammation

Incorporation of BrdU into the neointima cells was decreased in nutlin-3-treated mice compared with control mice at 14 days but not 28 days after vascular injury (*Figure 4A*). There were only a few TUNEL-positive apoptotic cells detected at 7 days after injury, however, enhanced apoptosis was not observed in nutlin-3-administered mice (*Figure 4B*). TUNEL-positive cells were not detected either in control or nutlin-3 groups at 14 and 28 days after injury (*Figure 4B*). These results suggest minor contribution of

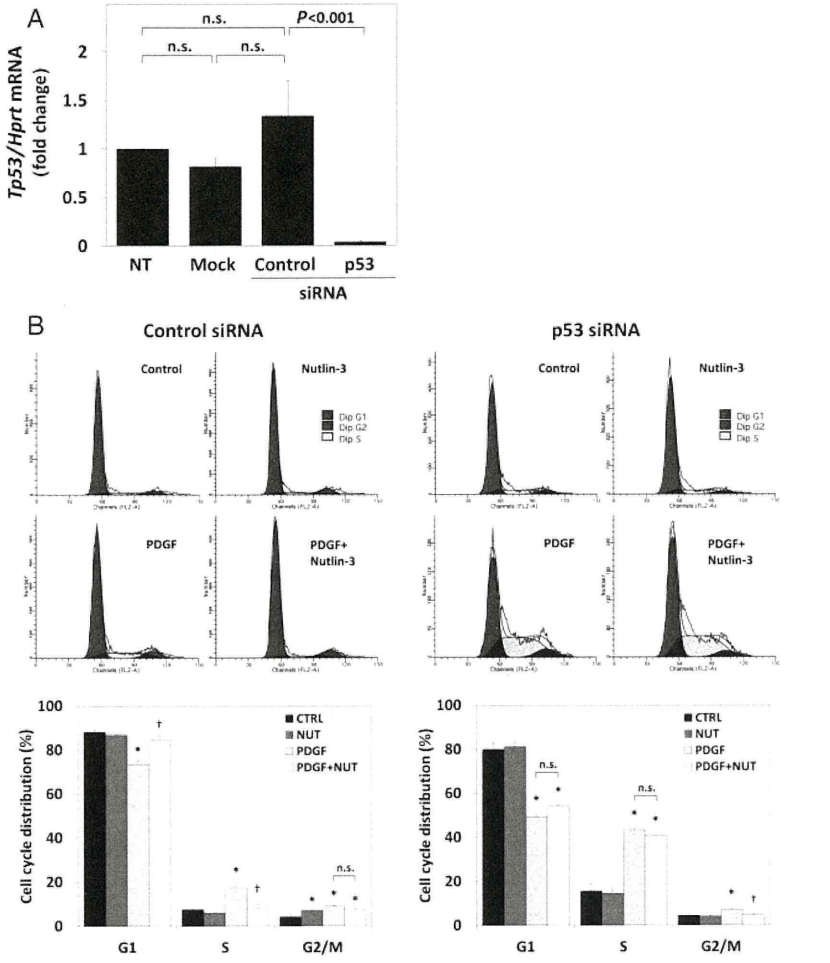

Figure 2 Nutlin-3 induces cell cycle arrest in a p53-dependent manner in VSMC. (*A*) The expression levels of p53 mRNA in VSMCs transfected with p53-targeting siRNA (25 nmol/L) or negative control siRNA (25 nmol/L) for 48 h were assessed by RT-qPCR ($n = 4$). NT, non-treated. n.s., not significant. (*B*) Cell cycle profile analysed by flow cytometry. VSMCs transfected with p53-siRNA (25 nmol/L) or control siRNA (25 nmol/L) were pretreated with nutlin-3 (10 μmol/L) for 6 h and then stimulated with PDGF-BB (50 ng/mL) for 24 h. Representative histograms and the percentage of cell cycle distribution are shown. CTRL, control, NUT, nutlin-3. $^{*}P < 0.05$ vs. control, $^{\dagger}P < 0.01$ vs. PDGF ($n = 3$ each).

apoptosis to the inhibition of neointimal growth by nutlin-3. Vascular inflammation is mainly regulated by NF-κB-dependent gene transcription,[22] and involved in the progression of vascular proliferative diseases.[1–3] Since it has been reported that p53 inhibits NF-κB pathway,[23–27] we also investigated whether nutlin-3 affects NF-κB-regulated gene expression and infiltration of inflammatory cells in injured vascular tissues. Infiltration of macrophages and T-lymphocytes in the injured vessels was significantly attenuated in nutlin-3-administered mice (*Figure 4C and D*). RT-qPCR of the injured vessels showed that mRNA expression of NF-κB-regulated genes including chemokine (C-C motif) ligand 5 (CCL5), interleukin-6 (IL-6), and intercellular adhesion molecule-1 (ICAM-1) was suppressed in nutlin-3-treated mice (*Figure 5A*).

3.5 Nutlin-3 suppression of nuclear activation of NF-κB is dependent on p53

To elucidate the mechanism of the decrease in proinflammatory gene expression in the injured vessels of nutlin-3-treated mice, we performed NF-κB DNA-binding ELISA using cultured rat VSMCs. Treatment with nutlin-3 significantly attenuated NF-κB activation induced by TNFα in VSMCs transfected with control siRNA (*Figure 5B*), while this inhibitory effect was abrogated in VSMCs transfected with p53-targeting siRNA (*Figure 5B*). The NF-κB-suppressing effect of nutlin-3 was also abolished in p53-deficient mouse VSMCs (Supplementary material online, *Figure S3*). These results suggest that the inhibitory effect of nutlin-3 on NF-κB activation depends on p53.

4. Discussion

In the present study, we demonstrated that an MDM2 inhibitor nutlin-3 suppressed VSMC proliferation through cell cycle arrest at G1 phase. The effects of nutlin-3 depend on p53 because nutlin-3 failed to show any effects on VSMCs transfected with p53-targeting siRNA and p53-deficient VSMCs. We also demonstrated that treatment with nutlin-3 attenuated neointimal hyperplasia after vascular injury without increasing vascular tissue vulnerability. Inhibition of

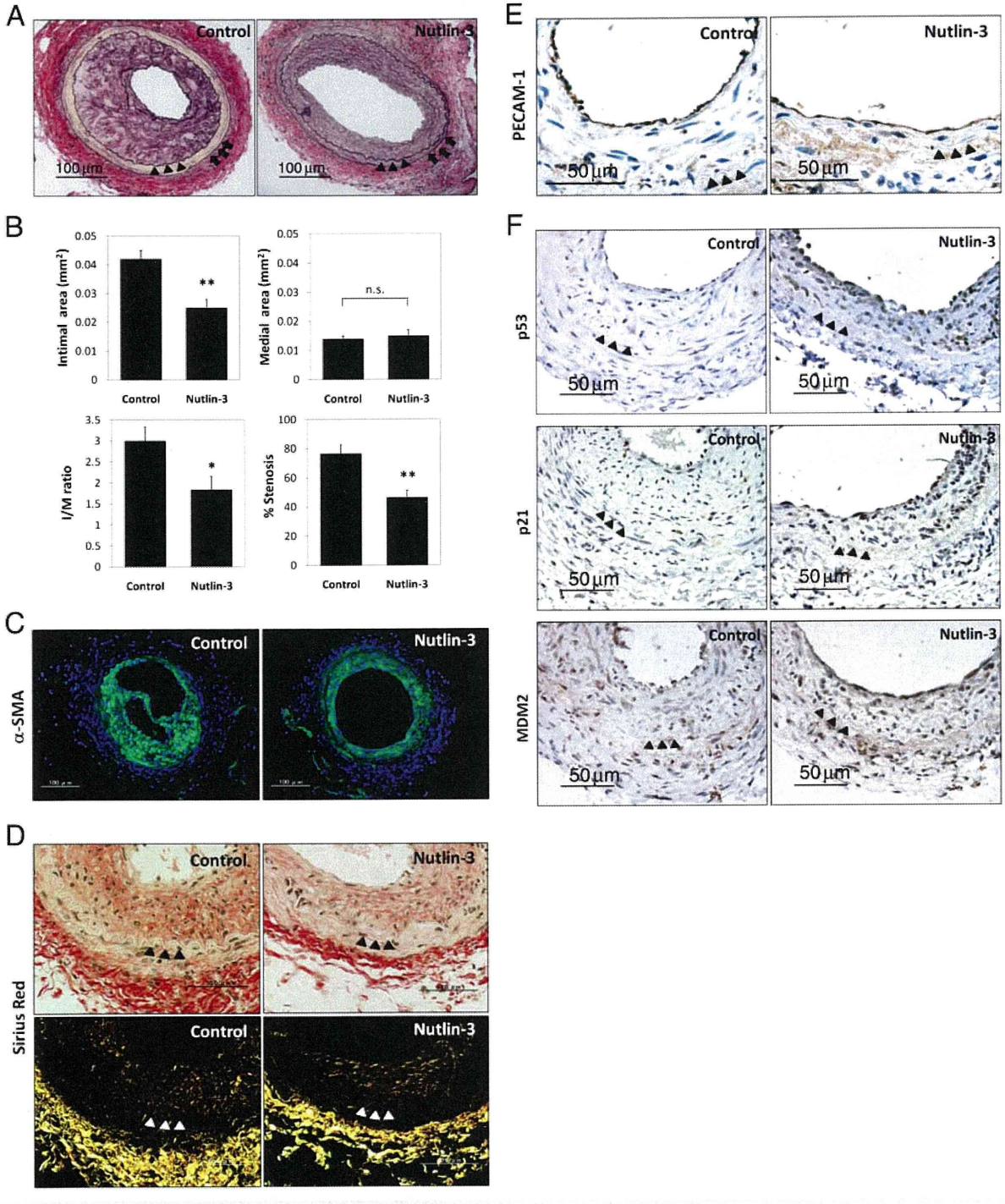

Figure 3 Nutlin-3 attenuates neointimal hyperplasia after vascular injury. (*A*) Femoral arteries at 28 days after vascular injury (elastica van Gieson staining). Arrows indicate external elastic lamina. Arrowheads indicate internal elastic lamina. (*B*) Intimal area, medial area, intima/media (I/M) area ratio, and percent stenosis at 28 days after injury were analysed. Values represent mean ± SEM. $^{*}P < 0.05$ vs. control, $^{**}P < 0.01$ vs. control (control, $n = 9$, nutlin-3, $n = 7$). (*C*) Wire-injured arteries (28 days) stained with FITC-conjugated anti-α-SMA antibody. Green, α-SMA. Blue, nuclei (DAPI). (*D*) Sirius red staining of injured vessels (28 days). Collagen fibres were stained in red (upper panels). The sirius red-stained tissue specimens identical to upper panels were observed by polarizing microscopy (lower panels). (*E*) Immunostaining of PECAM-1 in vascular tissues at 28 days after injury. (*F*) Immunostaining of p53, p21, and MDM2 in the injured vessels (28 days). The same results were obtained in other samples (control, $n = 9$, nutlin-3, $n = 7$).

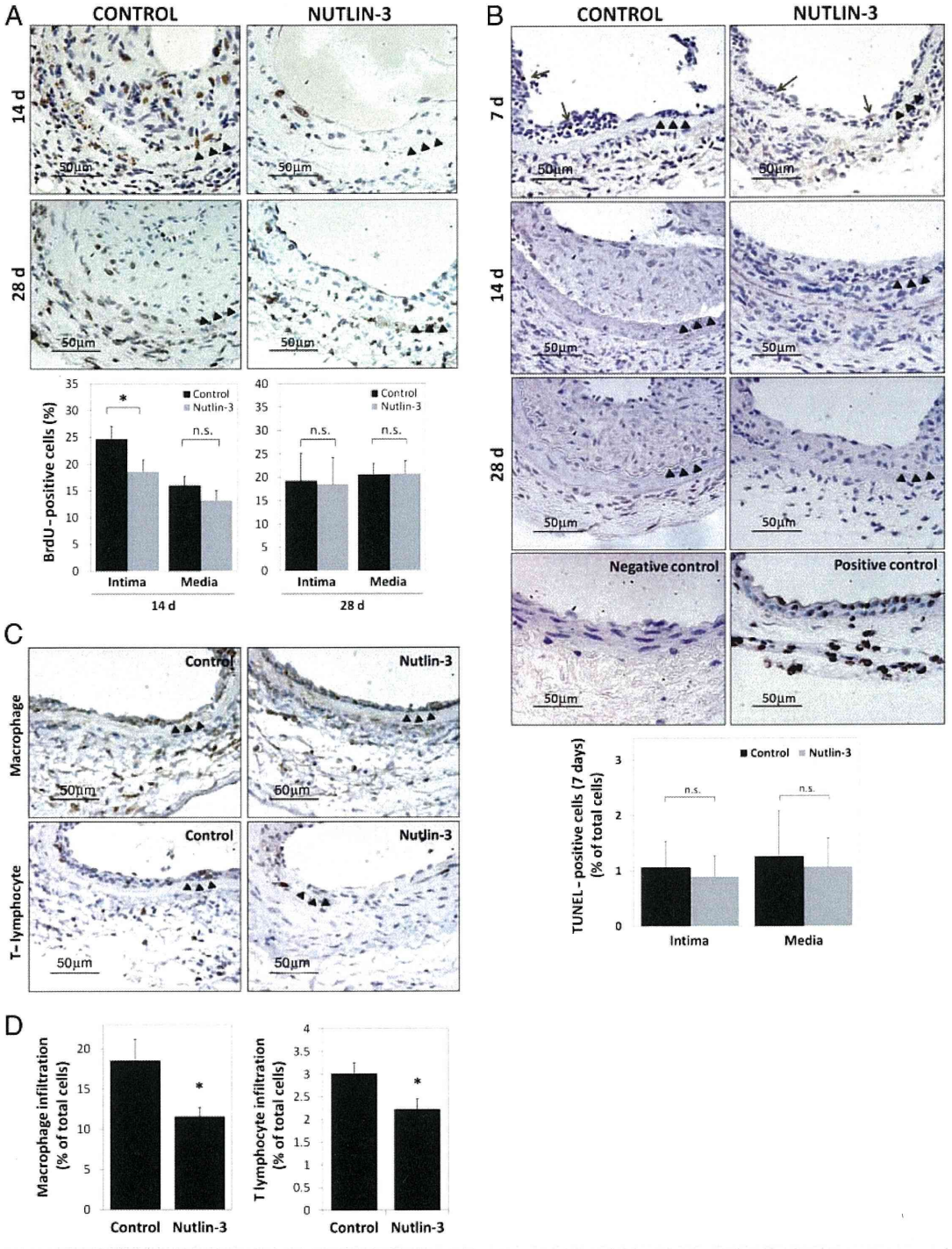

Figure 4 Modulation of vascular proliferation and inflammatory responses by MDM2 inhibition. (*A*) Cell proliferation was assessed by BrdU incorporation at 14 and 28 days after vascular injury. (Upper) Representative micrographs are shown. Arrowheads indicate internal elastic lamina. (Lower) Quantitative analysis of BrdU-positive cells in the neointima and the media. *$P < 0.05$. n.s.: not significant. (14 days: control, $n = 15$, nutlin-3, $n = 11$; 28 days: control, $n = 9$, nutlin-3, $n = 7$). (*B*) (Upper) Apoptotic cells assessed by TUNEL method at 7, 14, and 28 days after injury. Arrows indicate TUNEL-positive cells. Positive control was the tissue specimen biochemically treated with DNase I, while negative control was the specimen incubated without TdT. (Lower) Quantitative analysis of TUNEL-positive cells in the neointima and the media at 7 days after injury. n.s., not significant (control, $n = 7$, nutlin-3, $n = 8$). (*C*) Infiltration of inflammatory cells at 7 days after vascular injury. Macrophages were immunostained with anti-Mac-3 antibody. T-lymphocytes were stained with anti-CD3 antibody. (*D*) Quantitative analysis of the number of inflammatory cells which infiltrated per section. *$P < 0.05$ vs. control ($n = 5$ each).

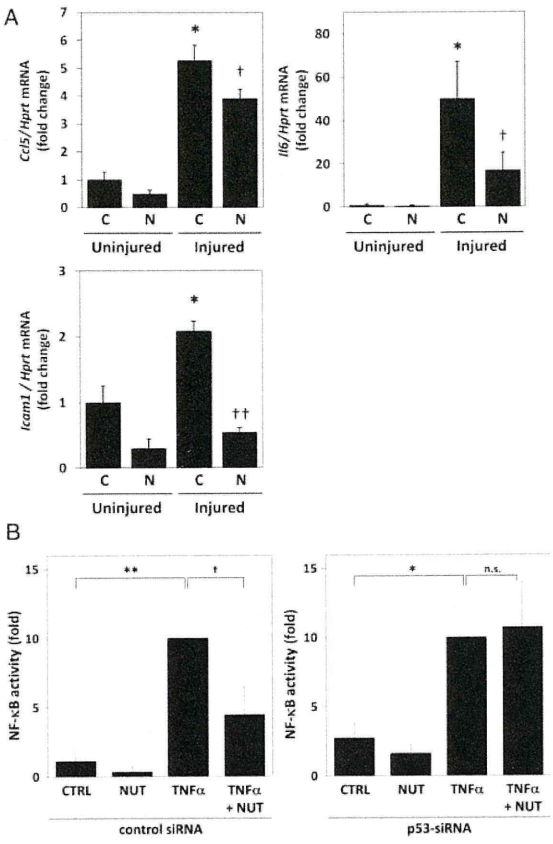

Figure 5 Effects of MDM2 inhibition on inflammatory gene expression and NF-κB transcriptional activity. (*A*) mRNA expression levels of CCL5, IL-6, and ICAM-1 at 7 days after vascular injury were determined by RT-qPCR. C, control; N, nutlin-3. $^{*}P < 0.005$ vs. control (uninjured); $^{\dagger}P < 0.05$, $^{\dagger\dagger}P < 0.01$ vs. control (injured) (control, $n = 10$, nutlin-3, $n = 10$). Values represent mean ± SEM. (*B*) Effect of nutlin-3 on NF-κB transactivation in VSMCs was assessed by DNA-binding ELISA for NF-κB p65. VSMCs transfected with control siRNA or p53-siRNA were stimulated with TNFα (20 ng/mL) for 1 h after pretreatment with nutlin-3 (10 μmol/L) for 24 h ($n = 3$ each). Values represent mean ± SEM. CTRL, control; NUT, nutlin-3. $^{*}P < 0.05$, $^{**}P < 0.001$ vs. control, $^{\dagger}P < 0.05$ vs. TNFα, n.s., not significant ($n = 3$).

vascular cell proliferation, inflammatory cell infiltration, and proinflammatory gene expression was observed in the injured vessels of nutlin-3-administered mice, suggesting that nutlin-3 ameliorated maladaptive vascular remodelling through inhibition of neointimal VSMC growth and modulation of inflammatory process. Infiltration of leukocytes mediated by chemokines and VSMC proliferation are critical to neointimal growth after vascular injury.[3] Therefore, a therapeutic strategy against both cell proliferation and vascular inflammation is rational for efficacious remedy for neointimal hyperplasia. MDM2 inhibitors may have unique therapeutic potential because it is capable of inhibiting NF-κB activation as well as inducing cell-cycle arrest via p53 activation.

Previous reports have demonstrated that the protective role of p53 against neointimal hyperplasia.[28–34] Such an effect has been thought to be brought about by increased apoptosis or inhibition of proliferation of VSMCs. These studies adopted, however, p53 gene transfer by adenovirus vectors, liposome, or transgenic technique, which are technically and ethically difficult to utilize in the clinical settings. Indeed p53 activation can be instigated by anticancer drugs, which is inevitably associated with DNA damage leading to enhanced apoptosis and tissue damage.[15] The fact that nutlin-3 can activate p53 by inhibition of MDM2, not by DNA damage-triggered induction, encourages us to apply the 'p53 activation' to the conquest of vascular proliferative diseases practically.

Since MDM2 is a downstream target gene of p53 as well as p21, MDM2 up-regulation by treatment with MDM2 inhibitor nutlin-3 is thought to result from a negative feedback mechanism. Although the kinetics of p53, p21, and MDM2 in VSMCs seems parallel in time in our results, up-regulation of p21 and MDM2 may follow the induction of p53 in a delayed fashion at the early phase after stimulation with nutlin-3 like seen in other cells.[18,19]

Nutlin-3 inhibits cell proliferation by p53 activation leading to p21-mediated cell cycle arrest at G1 phase. p53 can also induce apoptosis in response to stress signals, but apoptosis-inducing effect of p53 might depend on cell type or require further cofactors or modifications.[35] Nutlin-3 does not induce apoptosis of vascular endothelial cells,[36] neutrophils, and macrophages.[23] In this study, acceleration of apoptosis was not observed either in nutlin-3-treated VSMCs or neointima of nutlin-3-administered mice after vascular injury, which is consistent with previous studies. Very early apoptosis after vascular injury is relevant for vascular remodelling. SMC apoptosis is induced immediately after vascular injury, attaining to the peak in 0.5–1 h, and declines rapidly.[37] Considering the fact that administration of nutlin-3 was instituted by implantation of mini-osmotic pumps following vascular injury and the concentration of nutlin-3 would reach steady state for at least several hours, it is unlikely that nutlin-3 affects apoptosis which occurs very early after vascular injury in our models.

p53 activation is known to suppress NF-κB-dependent gene expression.[23–25] It has been reported that p53 and NF-κB can repress the transactivation of each other via competition for transcriptional co-activator p300/CREB-binding protein (CBP).[26,27] We showed that nutlin-3 suppressed NF-κB activation in VSMCs. Though a direct proof of NF-κB activation is lacking in our animal experiments, inhibition of the expression of NF-κB-regulated proinflammatory genes, such as CCL5, IL-6, and ICAM-1, suggests that nutlin-3 may suppress NF-κB activation in injured vessels as shown in cultured VSMCs. These observations about the effects of MDM2 inhibitor beyond anti-proliferation, that is, anti-inflammatory activities, implicate that it may be applicable to the treatment of atherosclerotic vascular diseases as well as post-intervention restenosis.

In the present study, we did not investigate the mechanism by which nutlin-3 suppressed VSMC migration. Nutlin-3 inhibits cancer cell migration via cytoskeletal rearrangement in a p53-dependent manner.[38] Reportedly, p53 inhibits cell migration by regulation of Cdc42 and Rac1 pathways.[39,40] While we speculate that nutlin-3 inhibits VSMC migration through p53-mediated suppression of Rho GTPases, further examination is required.

The limitation of the present study is that we did not verify the effects of nutlin-3 on neointima formation in p53-deficient mice to establish the definite link between the effects of nutlin-3 and p53 *in vivo*. However, we observed that nutlin-3 failed to inhibit cell cycle progression and NF-kB activation in p53-knocked down

VSMCs and p53-deficient VSMCs, strongly suggesting that the effects of nutlin-3 depend on p53. Furthermore, there are many reports demonstrating that *in vivo* administration of nutlin-3 suppressed the growth of tumours with wild-type p53, whereas treatment with nutlin-3 did not affect the growth of p53-deficient or mutant p53-bearing tumours in mice.[17,18,41] These findings including our results suggest that the pharmacological action of nutlin-3 *in vivo* is dependent on p53 as well. For another point, we cannot exclude possible secondary effects of nutlin-3 on neointima formation by way of, for example, inhibition of systemic cytokine expression and direct inhibitory effects on inflammatory cells such as macrophages and leukocytes. Further investigations are required on this point.

In conclusion, p53 activation by MDM2 inhibition prevented cellular proliferation, migration, and NF-κB activation in VSMCs; and besides attenuated neointimal hyperplasia with prevention of vascular proliferation and inflammatory responses. Targeting MDM2-p53 interaction might be a novel therapeutic strategy for treatment of vascular proliferative diseases.

Supplementary material

Supplementary material is available at *Cardiovascular Research* online.

Acknowledgements

We thank the Research Support Centre, Kyushu University Graduate School of Medical Sciences for technical supports.

Conflict of interest: none declared.

Funding

This work was supported in part by Grants-in-Aid for Scientific Research from the Ministry of Education, Culture, Sports, Science, and Technology of Japan (19590867).

References

1. Libby P. Inflammation in atherosclerosis. *Nature* 2002;**420**:868–874.
2. Dzau VJ, Braun-Dullaeus RC, Sedding DG. Vascular proliferation and atherosclerosis: new perspectives and therapeutic strategies. *Nat Med* 2002;**8**:1249–1256.
3. Costa MA, Simon DI. Molecular basis of restenosis and drug-eluting stents. *Circulation* 2005;**111**:2257–2273.
4. Riley T, Sontag E, Chen P, Levine A. Transcriptional control of human p53-regulated genes. *Nat Rev Mol Cell Biol* 2008;**9**:402–412.
5. Guevara NV, Kim HS, Antonova EI, Chan L. The absence of p53 accelerates atherosclerosis by increasing cell proliferation *in vivo*. *Nat Med* 1999;**5**:335–339.
6. van Vlijmen BJ, Gerritsen G, Franken AL, Boesten LS, Kockx MM, Gijbels MJ *et al.* Macrophage p53 deficiency leads to enhanced atherosclerosis in APOE*3-Leiden transgenic mice. *Circ Res* 2001;**88**:780–786.
7. Merched AJ, Williams E, Chan L. Macrophage-specific p53 expression plays a crucial role in atherosclerosis development and plaque remodeling. *Arterioscler Thromb Vasc Biol* 2003;**23**:1608–1614.
8. Mercer J, Figg N, Stoneman V, Braganza D, Bennett MR. Endogenous p53 protects vascular smooth muscle cells from apoptosis and reduces atherosclerosis in ApoE knockout mice. *Circ Res* 2005;**96**:667–674.
9. von der Thüsen JH, van Vlijmen BJ, Hoeben RC, Kockx MM, Havekes LM, van Berkel TJ *et al.* Induction of atherosclerotic plaque rupture in apolipoprotein E−/− mice after adenovirus-mediated transfer of p53. *Circulation* 2002;**105**:2064–2070.
10. Toledo F, Wahl GM. MDM2 and MDM4: p53 regulators as targets in anticancer therapy. *Int J Biochem Cell Biol* 2007;**39**:1476–1482.
11. Toledo F, Wahl GM. Regulating the p53 pathway: in vitro hypotheses, *in vivo* veritas. *Nat Rev Cancer* 2006;**6**:909–923.
12. Ihling C, Haendeler J, Menzel G, Hess RD, Fraedrich G, Schaefer HE *et al.* Co-expression of p53 and MDM2 in human atherosclerosis: implications for the regulation of cellularity of atherosclerotic lesions. *J Pathol* 1998;**185**:303–312.
13. Nakamura Y, Suzuki S, Suzuki T, Ono K, Miura I, Satoh F *et al.* MDM2: a novel mineralocorticoid-responsive gene involved in aldosterone-induced human vascular structural remodeling. *Am J Pathol* 2006;**169**:362–371.
14. Vassilev LT, Vu BT, Graves B, Carvajal D, Podlaski F, Filipovic Z *et al.* In vivo activation of the p53 pathway by small-molecule antagonists of MDM2. *Science* 2004;**303**:844–848.
15. Vassilev LT. MDM2 inhibitors for cancer therapy. *Trends Mol Med* 2007;**13**:23–31.
16. Sarek G, Kurki S, Enback J, Iotzova G, Haas J, Laakkonen P *et al.* Reactivation of the p53 pathway as a treatment modality for KSHV-induced lymphomas. *J Clin Invest* 2007;**117**:1019–1028.
17. Van Maerken T, Ferdinande L, Taildeman J, Lambertz I, Yigit N, Vercruysse L *et al.* Antitumor activity of the selective MDM2 antagonist nutlin-3 against chemoresistant neuroblastoma with wild-type p53. *J Natl Cancer Inst* 2009;**101**:1562–1574.
18. Tovar C, Rosinski J, Filipovic Z, Higgins B, Kolinsky K, Hilton H *et al.* Small-molecule MDM2 antagonists reveal aberrant p53 signaling in cancer: implications for therapy. *Proc Natl Acad Sci USA* 2006;**103**:1888–1893.
19. Endo S, Yamato K, Hirai S, Moriwaki T, Fukuda K, Suzuki H *et al.* Potent *in vitro* and *in vivo* antitumor effects of MDM2 inhibitor nutlin-3 in gastric cancer cells. *Cancer Sci* 2011;**102**:605–613.
20. Sata M, Maejima Y, Adachi F, Fukino K, Saiura A, Sugiura S *et al.* A mouse model of vascular injury that induces rapid onset of medial cell apoptosis followed by reproducible neointimal hyperplasia. *J Mol Cell Cardiol* 2000;**32**:2097–2104.
21. Andrae J, Gallini R, Betsholtz C. Role of platelet-derived growth factors in physiology and medicine. *Genes Dev* 2008;**22**:1276–1312.
22. de Winther MP, Kanters E, Kraal G, Hofker MH. Nuclear factor κB signaling in atherogenesis. *Arterioscler Thromb Vasc Biol* 2005;**25**:904–914.
23. Liu G, Park YJ, Tsuruta Y, Lorne E, Abraham E. p53 Attenuates lipopolysaccharide-induced NF-κB activation and acute lung injury. *J Immunol* 2009;**182**:5063–5071.
24. Dey A, Wong ET, Bist P, Tergaonkar V, Lane DP. Nutlin-3 inhibits the NFκB pathway in a p53-dependent manner: implications in lung cancer therapy. *Cell Cycle* 2007;**6**:2178–2185.
25. Secchiero P, Corallini F, Rimondi E, Chiaruttini C, di Iasio MG, Rustighi A *et al.* Activation of the p53 pathway down-regulates the osteoprotegerin expression and release by vascular endothelial cells. *Blood* 2008;**111**:1287–1294.
26. Wadgaonkar R, Phelps KM, Haque Z, Williams AJ, Silverman ES, Collins T. CREB-binding protein is a nuclear integrator of nuclear factor-κB and p53 signaling. *J Biol Chem* 1999;**274**:1879–1882.
27. Webster GA, Perkins ND. Transcriptional cross talk between NF-κB and p53. *Mol Cell Biol* 1999;**19**:3485–3495.
28. Yonemitsu Y, Kaneda Y, Tanaka S, Nakashima Y, Komori K, Sugimachi K *et al.* Transfer of wild-type p53 gene effectively inhibits vascular smooth muscle cell proliferation *in vitro* and *in vivo*. *Circ Res* 1998;**82**:147–156.
29. Matsushita H, Morishita R, Aoki M, Tomita N, Taniyama Y, Nakagami H *et al.* Transfection of antisense p53 tumor suppressor gene oligodeoxynucleotides into rat carotid artery results in abnormal growth of vascular smooth muscle cells. *Circulation* 2000;**101**:1447–1452.
30. George SJ, Angelini GD, Capogrossi MC, Baker AH. Wild-type p53 gene transfer inhibits neointima formation in human saphenous vein by modulation of smooth muscle cell migration and induction of apoptosis. *Gene Ther* 2001;**8**:668–676.
31. Mayr U, Mayr M, Li C, Wernig F, Dietrich H, Hu Y *et al.* Loss of p53 accelerates neointimal lesions of vein bypass grafts in mice. *Circ Res* 2002;**90**:197–204.
32. Sata M, Tanaka K, Ishizaka N, Hirata Y, Nagai R. Absence of p53 leads to accelerated neointimal hyperplasia after vascular injury. *Arterioscler Thromb Vasc Biol* 2003;**23**:1548–1552.
33. Wan S, George SJ, Nicklin SA, Yim AP, Baker AH. Overexpression of p53 increases lumen size and blocks neointima formation in porcine interposition vein grafts. *Mol Ther* 2004;**9**:689–698.
34. Sanz-González SM, Barquín L, García-Cao I, Roque M, González JM, Fuster JJ *et al.* Increased p53 gene dosage reduces neointimal thickening induced by mechanical injury but has no effect on native atherosclerosis. *Cardiovasc Res* 2007;**75**:803–812.
35. Aylon Y, Oren M. Living with p53, dying of p53. *Cell* 2007;**130**:597–600.
36. Secchiero P, Corallini F, Gonelli A, Dell'Eva R, Vitale M, Capitani S *et al.* Antiangiogenic activity of the MDM2 antagonist nutlin-3. *Circ Res* 2007;**100**:61–69.
37. Perlman H, Maillard L, Krasinski K, Walsh K. Evidence for the rapid onset of apoptosis in medial smooth muscle cells after balloon injury. *Circulation* 1997;**95**:981–987.
38. Moran DM, Maki CG. Nutlin-3a induces cytoskeletal rearrangement and inhibits the migration and invasion capacity of p53 wild-type cancer cells. *Mol Cancer Ther* 2010;**9**:895–905.
39. Gadea G, Lapasset L, Gauthier-Rouviere C, Roux P. Regulation of Cdc42-mediated morphological effects: a novel function for p53. *Embo J* 2002;**21**:2373–2382.
40. Guo F, Gao Y, Wang L, Zheng Y. p19Arf-p53 tumor suppressor pathway regulates cell motility by suppression of phosphoinositide 3-kinase and Rac1 GTPase activities. *J Biol Chem* 2003;**278**:14414–14419.
41. Sur S, Pagliarini R, Bunz F, Rago C, Diaz LA Jr., Kinzler KW *et al.* A panel of isogenic human cancer cells suggests a therapeutic approach for cancers with inactivated p53. *Proc Natl Acad Sci USA* 2009;**106**:3964–3969.

Peak Systolic Mitral Annulus Velocity Reflects the Status of Ventricular-Arterial Coupling—Theoretical and Experimental Analyses

Kazunori Uemura, MD, PhD, Toru Kawada, MD, PhD, Kenji Sunagawa, MD, PhD, and Masaru Sugimachi, MD, PhD, *Suita and Fukuoka, Japan*

Background: Peak systolic mitral annular velocity (S_m) measured by tissue Doppler echocardiography has been recognized as an independent predictor of mortality in patients with heart failure and in the general population. However, the mechanical determinants of S_m remain poorly defined.

Methods: A theoretical model of S_m was derived, which indicates that S_m is affected positively by left ventricular (LV) contractility and preload and inversely by LV afterload and ejection time (EJT). In 16 anesthetized dogs, S_m, LV volume, and LV pressure were measured using sonomicrometry and catheter-tip micromanometry. LV contractility, preload, and afterload were indexed by the end-systolic pressure/volume ratio (E_{es}'), end-diastolic volume (V_{ed}), and effective arterial elastance (E_a), respectively. LV contractility, loading conditions, and heart rate were varied over wide ranges, and a total of 76 data sets were obtained for S_m (1.2–9.1 cm/sec), E_{es}' (1.5–17.6 mm Hg/mL), V_{ed} (11–99 mL), E_a (3.6–58.4 mm Hg/mL), EJT (100–246 msec), heart rate (66–192 beats/min), and the ventricular-arterial coupling ratio (E_{es}'/E_a; 0.2–3.0).

Results: The theoretical model accurately predicted S_m ($R^2 = 0.79$, $P < .0001$). By univariate analysis, S_m was correlated significantly with E_{es}' ($R^2 = 0.64$, $P < .0001$) and with the reciprocal of E_a ($R^2 = 0.49$, $P < .01$). V_{ed} and EJT did not affect S_m. E_{es}'/E_a was correlated strongly with S_m ($R^2 = 0.73$, $P < .0001$). E_{es}' and the reciprocal of E_a were not correlated with each other.

Conclusions: LV contractility and afterload independently determine S_m. The effects of LV preload and EJT on S_m might be small, even though they are theoretically associated with S_m. S_m strongly reflects the status of ventricular-arterial coupling. (J Am Soc Echocardiogr 2011;24:582-91.)

Keywords: Echocardiography, Heart failure, Hemodynamics, Mechanics

Left ventricular (LV) longitudinal shortening during ejection is reflected by systolic mitral annular velocity, which can be measured by tissue Doppler (TD) echocardiography in clinical practice.[1] Peak systolic mitral annular velocity (S_m) has been reported to be an index of global LV systolic function.[2,3] Measurement of S_m allows the detection of cardiac dysfunction more sensitively than the evaluation of other conventional LV function indexes, such as LV ejection fraction (LVEF).[4] S_m is a powerful prognosticator of mortality in patients with heart failure[5] and in the general population.[6] Although these previous studies have highlighted the clinical utility of S_m measurement, the mechanical determinants of S_m remain poorly defined.

S_m is correlated positively with LVEF in patients with cardiac diseases.[2] A recent animal study demonstrated that S_m is correlated with the maximum value of the time derivative of LV pressure (LVP) (LV dP/dt_{max}), an indicator of LV systolic function.[7] These findings suggest that LV contractility contributes significantly to S_m. However, the magnitudes of LVEF and dP/dt_{max} change in response to alteration in loading conditions, even if the intrinsic LV contractility is preserved.[8] Intriguingly, S_m and LV end-systolic elastance (E_{es}; a relatively load independent index of LV contractility) were found not to be correlated in patients with hypertension.[9] Henein *et al.*[10] assessed the effects of acute alterations in afterload on S_m during peripheral vascular surgery and reported that an increase in afterload by aortoiliac clamping decreased S_m. In contrast, in patients undergoing cardiac surgery, S_m was insensitive to changes in afterload after infusions of vasoactive agents.[11]

Whether and to what degree LV contractility and loading conditions independently affect S_m remain controversial. A more comprehensive approach is required to address this issue. The purpose of this study was to clarify the mechanisms that regulate the magnitude of S_m. To that end, we first derived the theoretical relationship between S_m and cardiovascular parameters describing LV contractility,

From the Department of Cardiovascular Dynamics, National Cerebral and Cardiovascular Center Research Institute, Suita, Japan (K.U., T.K., M.S.); and the Department of Cardiovascular Medicine, Kyushu University Graduate School of Medical Sciences, Fukuoka, Japan (K.S.).

This work was supported by a grant-in-aid for scientific research (C-20500404) from the Ministry of Education, Culture, Sports, Science and Technology and by the Intramural Research Fund (22-1-5) for Cardiovascular Diseases of the National Cerebral and Cardiovascular Center.

Reprint requests: Kazunori Uemura, MD, PhD, Department of Cardiovascular Dynamics, National Cerebral and Cardiovascular Center Research Institute, 5-7-1 Fujishirodai, Suita 565-8565, Japan (E-mail: *kuemura@ri.ncvc.go.jp*).

0894-7317/$36.00

doi:10.1016/j.echo.2011.01.010

Abbreviations

CV = Coefficient of variation

E_a = Effective arterial elastance

E_{es} = End-systolic elastance

EJT = Ejection time

HR = Heart rate

LV = Left ventricular

LVEF = Left ventricular ejection fraction

LVP = Left ventricular pressure

LVV = Left ventricular volume

P_{es} = End-systolic pressure

S_m = Peak systolic mitral annular velocity

S_{mTD} = Peak systolic myocardial velocity on tissue Doppler echocardiography

SV = Stroke volume

SVR = Systemic vascular resistance

TD = Tissue Doppler

V_{ed} = End-diastolic volume

V_{es} = End-systolic volume

afterload, and preload. Second, in canine experiments, we simultaneously acquired LVP, LV volume (LVV), and S_m using a catheter-tipped micromanometer and sonomicrometer, while varying LV contractility and loading conditions over wide ranges. We compared these experimental data with the theoretical predictions and evaluated the independent effects of the parameters on S_m.

METHODS

Theoretical Relationship Between S_m and Cardiovascular Parameters

We based our theoretical modeling on the LVP-LVV framework,[12] as shown in Figure 1. E_{es}, the slope of the relationship between end-systolic pressure (P_{es}) and end-systolic volume (V_{es}), is an index of LV contractility (Figure 1A). Effective arterial elastance, E_a, the slope of the relationship between P_{es} and stroke volume (SV), is an index of LV afterload.[13] The time-elastance curve of the left ventricle has a distinct waveform (Figure 1B).[14,15] The time-elastance curve during systole can be approximated to two straight lines, one for the isovolumic contraction phase and the other for the ejection phase (Figure 1B).[14,15] S_m is related to E_{es}, E_a, LV end-diastolic volume (V_{ed}) and ejection time (EJT) by the following formula:

$$S_m = \frac{\alpha}{3} \cdot \frac{E_{es}}{E_a} \cdot \frac{V_{ed}^{1/3}}{EJT}, \quad (1)$$

where α is a constant determined by the ratio of LV longitudinal to short-axis length. Details of the mathematical derivation of equation 1 are provided in the Appendix.

Animal Experiments

We used 22 adult mongrel dogs (both sexes; weight, 20–30 kg). The investigation conformed with the *Guide for the Care and Use of Laboratory Animals*.[16] All protocols were approved by the Animal Subjects Committee of the National Cerebral and Cardiovascular Center.

Experiment 1: Comparison of Mitral Annular Velocities Measured by Sonomicrometry and TD Echocardiography

Preparation. Six animals were used. After anesthesia was induced with sodium pentobarbital (25 mg/kg), the animals were intubated endotracheally and ventilated artificially. An appropriate level of anesthesia was maintained by continuous inhalation of 1.5% isoflurane. A sterile left lateral thoracotomy was performed, and the pericardium was opened. Three spheric sonomicrometer crystals (2 mm in diameter) were implanted in the subepicardium at the base (Figure 2A, points 1 and 2) and apex (Figure 2A, point 3) of the left ventricle. All wires were exteriorized through the back of the neck. The pericardium and chest wall were closed, and the animal was allowed to recover.

After the animals had fully recovered from the procedure (10–14 days after surgery), mitral annular velocities were measured by sonomicrometry and TD echocardiography. During measurements, the dogs were anesthetized and artificially ventilated and were laid in a sling. Surface electrocardiograms were recorded.

Mitral Annular Velocity Measurement by Sonomicrometry. To obtain LV dimensions, sonomicrometric signals were processed with a digital system (Sonolab, Sonometrics Corporation, London, Canada) while each crystal sent a signal to and received a signal from each of the other crystals. Analog signals of sonomicrometric LV dimensions and electrocardiography were digitized at 200 Hz and stored for offline analysis (Sonolab). The dimensions of the three sonomicrometer crystals were used to calculate the LV longitudinal length (L), which is the distance between the LV apex and the center of the base (Figure 2A). The time derivative of L (dL/dt) was used as instantaneous mitral annular velocity, and a positive velocity was reported to indicate shortening of L.[17] Peak dL/dt during LV systole was used as S_m.

Mitral Annular Velocity Measurement by TD Echocardiography. Transthoracic echocardiography was performed using an echocardiographic system equipped with a 6-MHz transducer (Artida; Toshiba Corporation, Tokyo, Japan). Mitral annular velocity was obtained with pulsed TD from the apical four-chamber view by placing a 2-mm-wide sample volume at the septal side of the mitral annulus (Figure 2B).[3] Peak systolic myocardial velocity (S_{mTD}) was obtained.[3,5]

Data Acquisition. All data were acquired at end-expiration. To avoid interference between sonomicrometry and TD echocardiography, we first recorded echocardiographic data for 10 sec and then sonomicrometric dimensions during the subsequent 10 sec. Doses of dobutamine (2, 4, 8, and 16 μg/kg/min) and propranolol (0.2 mg/kg) were administered intravenously to each dog to modulate LV inotropy. S_m and S_{mTD} were determined after administration of each dose.

Experiment 2: Effects of Cardiovascular Parameters on S_m

Preparation. Sixteen animals were used. Anesthesia and artificial ventilation were conducted as described above. A fluid-filled catheter (8Fr) was placed in the right femoral artery to measure systemic arterial pressure. The fluid-filled catheter was connected to a pressure transducer (DX-200; Nihon Kohden, Tokyo, Japan). After a median sternotomy, the heart was suspended in a pericardial cradle. A pair of pacing electrodes was fixed at the right atrial appendage for atrial pacing. A catheter-tipped micromanometer (PC-751; Millar Instruments, Houston, TX) was inserted via the LV apex to measure LVP. As depicted in Figure 3A, 10 sonomicrometer crystals were implanted in the subepicardium of the left ventricle and the right side of the interventricular septum to obtain LV dimensions. Surface electrocardiograms were recorded. After the instrumentation was completed, the pericardium was closed. All data acquisitions were done at end-expiration. Analog signals of arterial pressure, LVP,

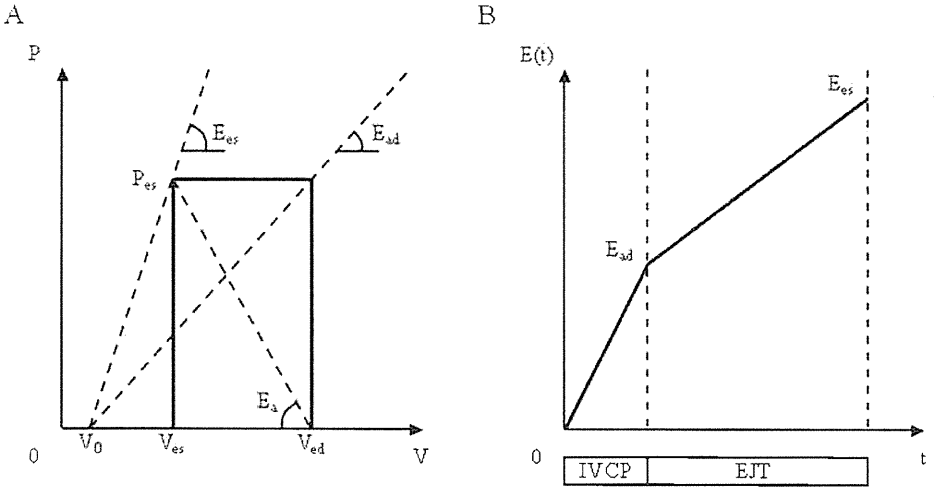

Figure 1 **(A)** Schematic drawing of the LVP (P)–LVV (V) loop, depicting E_{es}, E_{ad}, E_a, P_{es}, volume axis intercept of the relationship between P_{es} and V_{es} (V_0), V_{es}, and V_{ed}. **(B)** Bilinearly approximated time (*t*)–elastance (E[*t*]) curve during the isovolumic contraction phase (IVCP) and EJT.

sonomicrometric LV dimensions, and electrocardiography were digitized at 200 Hz and stored for offline analysis.

Experimental Protocols. After the initial preparation and surgical procedures were complete, the animals were allowed to stabilize for 30 min. Under steady-state baseline condition, we recorded the analog signals for about 10 sec in each animal. After obtaining the hemodynamic data at baseline conditions, we created various hemodynamic conditions, as described in the following protocols. In each protocol, we waited 20 min to confirm that hemodynamic conditions reached steady state.

Contractility Run (n = 9). —Hemodynamic data were recorded while LV contractility was increased by dobutamine infusion (5 μg/kg/min). After the data were recorded, dobutamine infusion was temporarily suspended. We created acute heart failure by embolizing the left coronary artery with glass microspheres (90 μm in diameter). Data recording was repeated under depressed LV contractility. Hemodynamic data were also recorded after LV contractility was restored by reinfusion of dobutamine.

Loading Run (n = 7). —Hemodynamic data were recorded after pharmacologically altering vascular resistance (afterload) and LV filling (preload) by infusing norepinephrine (0.2 μg/kg/min), sodium nitroprusside (3 μg/kg/min), or 250 mL of 10% dextran 40.

Heart Rate (HR) Run (n = 6). —The possible dependence of S_m on HR was tested by suppressing the intrinsic atrial beat using zatebradine (UL-FS49; 0.5 mg/kg) and instituting atrial pacing to obtain hemodynamic data at different HRs (±25% of baseline HR).

Six animals underwent both loading and HR runs. At the conclusion of the experiments, the dogs were sacrificed with an intravenous injection of pentobarbital and potassium chloride. Autopsies were performed to verify the position of the sonomicrometer crystals and catheters. After excision of the adjacent right ventricular muscle, valvular tissue and fat, LV myocardial volume was measured by water displacement in a volumetric cylinder.

Data Analysis and Definitions. *Calculation of S_m.* —Dimensions between the sonomicrometer crystals placed at the LV base (Figure 3A, points 1 and 2) and the LV apex (Figure 3A, point 3) were used to calculate S_m, as described above.

LVV Calculation Using Sonomicrometric LV Dimensions. —The three-dimensional position of each crystal was defined as a function of time on the basis of the distances between the crystals.[18] The LV epicardial volume (including LVV and LV myocardial volume) was estimated using software that applied an ellipsoidal shell model to the coordinates of all 10 crystals (Figure 3A).[19] LVV was obtained by subtracting LV myocardial volume from the estimated LV epicardial volume. Our preliminary study demonstrated that ex vivo LVV thus estimated agreed reasonably well with the volume measured by intraventricular balloon method (LVV_{ba}) in four canine hearts ($LVV = 1.0 \times LVV_{ba} - 7.0$; $r = 0.98$; SEE = 14 mL; $20 \leq LVV_{ba} \leq 70$ mL).

Cardiovascular Parameters. —End-systole was defined as the time when LV dP/dt decreased to 20% of its minimum.[15] LV contractility was indexed by the P_{es}/V_{es} ratio ($E_{es}' = P_{es}/V_{es}$), which is an approximation of E_{es}.[9,20] V_{ed} (an index of LV preload) was defined as LVV at the peak of the R wave on the electrocardiogram.[11] E_a (an index of LV afterload) was defined as the ratio of P_{es} to SV ($SV = V_{ed} - V_{es}$).[9,13] The end of the isovolumic contraction phase was defined as the moment when LV dP/dt decreased to 80% of its maximum, according to a previous study[21] with minor modification. EJT was obtained by subtracting the end of the isovolumic contraction phase from end-systole. Systemic vascular resistance (SVR) was defined as time-averaged arterial pressure divided by the product of SV and HR. A previous study demonstrated that E_a is related to SVR and HR as follows: $E_a \approx k \times SVR \times HR$, where k is a constant.[13] The E_{es}'/E_a ratio was used as an index of ventricular-arterial coupling.[14,20]

S_m and cardiovascular parameters were the averages of approximately 10 beats.

Statistical Analysis

All data are presented as mean ± SD. Statistical analyses were performed using commercially available software (Statistica; Statsoft, Inc., Tulsa, OK). In experiments 1 and 2, the associations among variables were analyzed using a mixed-model procedure to handle the dependencies in repeated measurements within the same animal.[7,17,22,23] The coefficient of determination (R^2) was used to evaluate the strength of association, because it measures how much variability of the dependent variable is the result of the independent

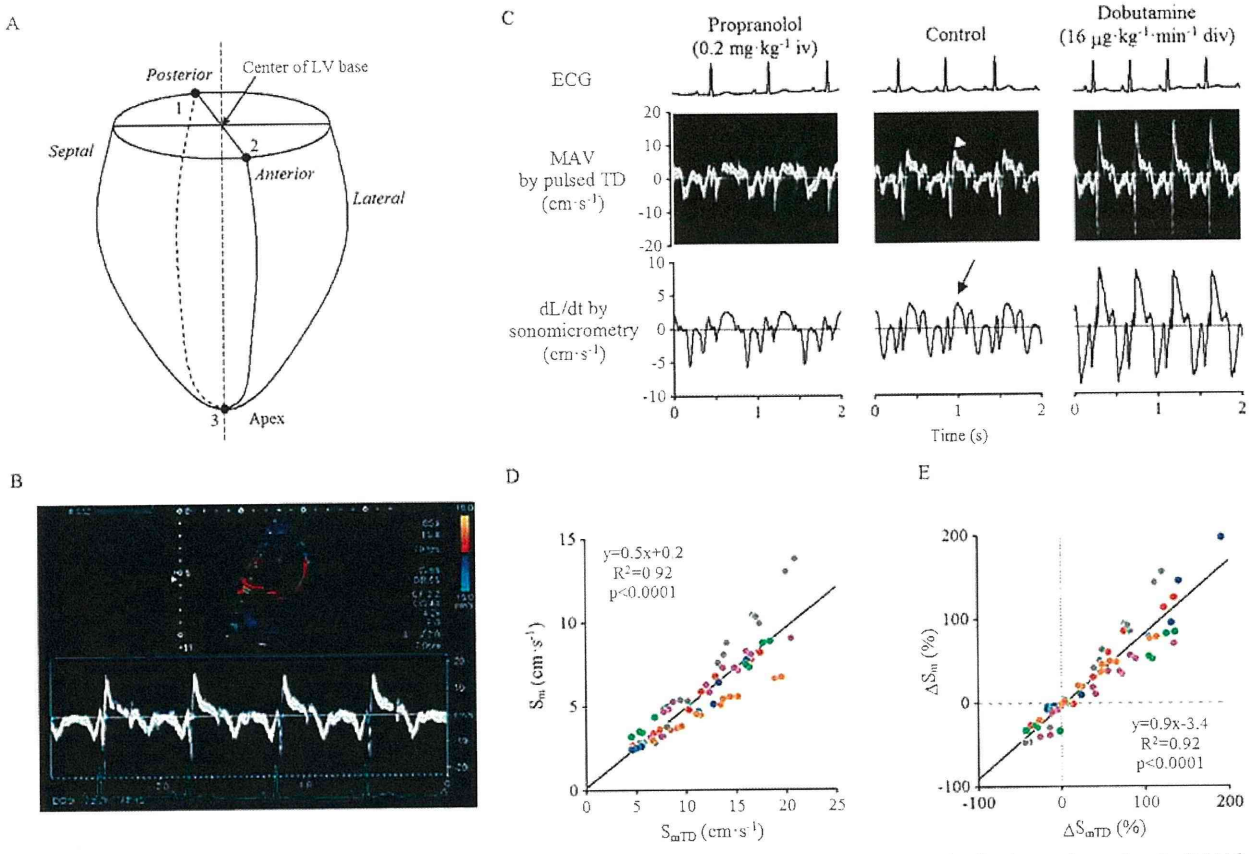

Figure 2 **(A)** Placement of sonomicrometer crystals (see text) in experiment 1. **(B)** Measurement of mitral annular velocity (MAV) at the septal side of the mitral annulus by TD echocardiography. **(C)** Examples of waveform data of electrocardiogram, septal MAV obtained from TD echocardiography, and dL/dt measured by implanted sonomicrometer crystals during hemodynamic alterations induced by dobutamine and propranolol. Data for dL/dt were traced so that positive values indicated shortening of LV longitudinal length.[17] Because of interference between sonomicrometry and Doppler, TD velocities were not from the same heartbeat as the other recordings. *Arrowhead*, S_{mTD}; *arrow*, S_m. **(D)** Relation between S_m and S_{mTD} in six dogs. Each *color* indicates the data from one animal. The line represents the population-averaged regression[20] between S_m and S_{mTD} with regression equation, coefficient of determination (R^2), and probability value. **(E)** Relation between percentage changes in S_m (ΔS_m) and S_{mTD} (ΔS_{mTD}) from their respective baseline values in six dogs. Each color indicates the data from one animal. The *line* represents the population-averaged regression between ΔS_m and ΔS_{mTD} with regression equation, R^2, and probability value.

variable.[7] In experiment 2, the coefficient of variation (CV) was calculated as the ratio of the SD to the mean (reported as a percentage) and used to quantify the variability of measurements. One-way repeated-measures analyses of variance with Dunnett's test were used in multiple comparisons relative to baseline for each intervention. P values $< .05$ were considered statistically significant.

RESULTS

Experiment 1: Mitral Annular Velocity Measured by Sonomicrometry and TD Echocardiography

Figure 2C displays representative recordings of mitral annular velocity measured by TD echocardiography and dL/dt measured by sonomicrometry when LV contractility was pharmacologically modulated. Waveforms derived from TD echocardiography were slightly different from those derived from sonomicrometry. As shown in Figure 2D, the values of S_{mTD} were consistently larger than those of S_m, but the two were correlated strongly on the basis of the data obtained from six canine hearts over a wide range of LV inotropy ($R^2 = 0.92$). Percentage change in S_{mTD} was also correlated highly with percentage change in S_m ($R^2 = 0.92$; Figure 2E). On the basis of these findings, instead of S_{mTD}, we used S_m by sonomicrometry to investigate the mechanical determinants of systolic mitral annular velocity, because this allowed analyses of all variables, including LVP and LVV, from the same heartbeat.

Experiment 2: Effects of Cardiovascular Parameters on S_m

Figure 3B shows traces of hemodynamic variables in one animal under baseline conditions. As predicted in our theoretical analysis (Appendix), S_m was detected early in the ejection phase.

Effects of Various Interventions on S_m and Cardiovascular Parameters. Table 1 summarizes the effects of various interventions on S_m and cardiovascular parameters (a total of 76 data sets). The CVs for S_m, E_{es}', V_{ed}, E_a, EJT, SVR, HR, and E_{es}'/E_a were 44%, 49%, 41%, 77%, 24%, 77%, 21%, and 64%, respectively. S_m and all the cardiovascular parameters changed over reasonably wide ranges by the interventions.

Contractility Run. — S_m, E_{es}', and E_{es}'/E_a changed in a similar pattern from their respective baseline values. They increased significantly with

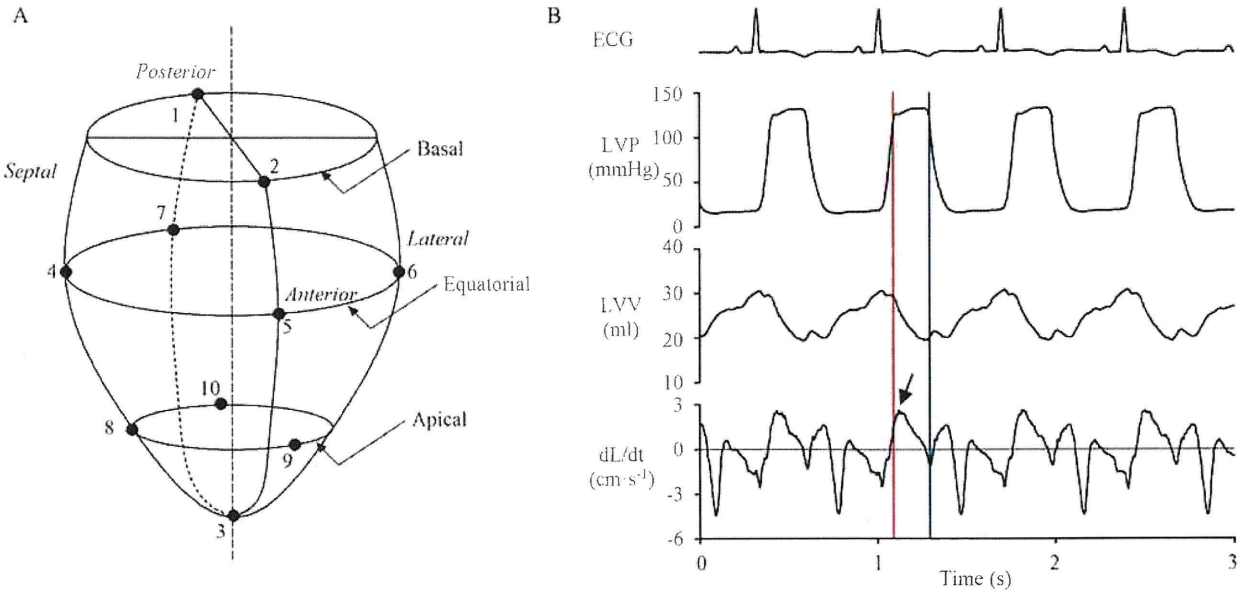

Figure 3 **(A)** Placement of sonomicrometer crystals (see text) in experiment 2. **(B)** Representative tracings from a dog in baseline condition. *Vertical red line*, end of isovolumic contraction phase; *vertical blue line*, end-systole; *arrow*, S_m.

dobutamine infusion, decreased significantly after acute heart failure induction, and recovered to baseline levels with reinfusion of dobutamine. V_{ed} and E_a significantly increased and EJT significantly decreased from their respective baseline values after acute heart failure induction.

Loading Run.—S_m, E_{es}', and E_{es}'/E_a did not change significantly in response to changes in loading conditions. Norepinephrine infusion significantly increased E_a and SVR and significantly decreased HR. Sodium nitroprusside infusion significantly decreased V_{ed} but did not significantly reduce E_a and SVR. Dextran infusion significantly increased V_{ed} and EJT and significantly decreased E_a and HR.

HR Run.—Zatebradine infusion significantly decreased HR and E_{es}' and significantly increased V_{ed} and EJT. Atrial tachypacing significantly increased HR. E_a was apparently decreased by zatebradine and increased by atrial tachypacing, although the differences were not significant.

Relationships Between S_m and Cardiovascular Parameters. Using the 76 data sets from all interventions, we examined whether S_m was related to the cardiovascular parameters as predicted by equation 1. As shown in Figure 4A, S_m was correlated significantly with the product of E_{es}' and the cubic root of V_{ed} divided by E_a and EJT. The R^2 value was 0.79, indicating that the theoretical model accurately predicts S_m.

Figures 4B to 4H shows univariate relationships between S_m and each of the cardiovascular parameters. S_m was correlated significantly with E_{es}' (Figure 4B). In accordance with equation 1, we related S_m with the cubic root of V_{ed} ($V_{ed}^{1/3}$; Figure 4C), with the reciprocal of E_a (E_a^{-1}; Figure 4D), and with the reciprocal of EJT (EJT^{-1}; Figure 4E). The CVs for E_a^{-1}, $V_{ed}^{1/3}$, and EJT^{-1} were 41%, 14%, and 21%, respectively. S_m was correlated significantly with E_a^{-1} but not with $V_{ed}^{1/3}$ and EJT^{-1}. Because E_a was correlated linearly with the product of SVR and HR, as described above, we related S_m with the reciprocal of SVR (SVR^{-1}; Figure 4F) and with the reciprocal of HR (HR^{-1}; Figure 4G). S_m was correlated significantly with SVR^{-1} but not with HR^{-1}. Figure 4H indicates that E_{es}'/E_a was tightly correlated with S_m.

We analyzed the correlations between the cardiovascular parameters. E_{es}' was not correlated with E_a^{-1} ($P = .96$), indicating that the two affect S_m independently. E_{es}' was correlated inversely with $V_{ed}^{1/3}$ ($E_{es}' = -4.3 \times V_{ed}^{1/3} + 21.7$; $R^2 = 0.56$, $P < .001$). E_a^{-1} was correlated inversely with EJT^{-1} ($E_a^{-1} = -0.03 \times EJT^{-1} + 0.34$; $R^2 = 0.76$, $P < .0001$). E_a^{-1} was correlated positively with $V_{ed}^{1/3}$ ($E_a^{-1} = 0.05 \times V_{ed}^{1/3} + 0.03$; $R^2 = 0.68$, $P < .01$). $V_{ed}^{1/3}$ was correlated inversely with EJT^{-1} ($V_{ed}^{1/3} = -0.16 \times EJT^{-1} + 4.45$; $R^2 = 0.76$, $P < .001$).

DISCUSSION

To the best of our knowledge, this is the first study to comprehensively evaluate the relations between S_m and cardiovascular parameters using theoretical modeling and also well-controlled animal experiments. The theoretical model of S_m indicates that S_m is affected by LV contractility, preload, afterload, and EJT. Experimental data confirmed that the theoretical model accurately predicts S_m. Further analysis of the experimental data showed that LV contractility and afterload have independent effects on S_m, but LV preload and EJT do not. S_m strongly reflects the status of ventricular-arterial coupling.

Mechanical Determinants of S_m

The theoretical model of S_m is rational mechanically because the right side of equation 1 corresponds to the mean velocity of LV shortening. The product of E_{es}/E_a and V_{ed} positively correlates with SV.[13] Therefore, the product of E_{es}/E_a and the cubic root of V_{ed}, which corresponds to LV end-diastolic dimension, positively correlates with the stroke dimension of the left ventricle. The stroke dimension of the left ventricle divided by EJT equals the mean velocity of LV shortening.

In our theoretical analysis, we assumed that changes in LV length couple with changes in LVV (Appendix). Actually, this is not the case throughout the cardiac cycle. In the isovolumic contraction

Table 1 Effect of interventions on systolic mitral annular velocity and cardiovascular parameters

Variable	S_m (cm/sec) 3.3 ± 1.5 (1.2–9.1)	E_{es}' (mm Hg/mL) 7.5 ± 3.7 (1.5–17.6)	V_{ed} (mL) 37 ± 16 (11–99)	E_a (mm Hg/mL) 9.2 ± 7.1 (3.6–58.4)	EJT (msec) 150 ± 36 (100–246)	SVR (mm Hg/sec/mL) 4.4 ± 3.3 (1.3–21.4)	HR (beats/min) 130 ± 28 (66–192)	E_{es}'/E_a 1.0 ± 0.7 (0.2–3.0)	*n* 76
Contractility run									
Baseline	3.4 ± 1.2	6.2 ± 1.7	38 ± 9	6.7 ± 1.4	134 ± 12	2.9 ± 0.7	130 ± 11	1.0 ± 0.4	9
DOB	6.0 ± 1.8†	10.5 ± 3.7†	45 ± 5	6.1 ± 1.6	127 ± 8	2.7 ± 1.1	136 ± 24	1.9 ± 0.9†	9
AHF	2.2 ± 1.0*	2.7 ± 0.8†	50 ± 17†	8.4 ± 2.4*	121 ± 13†	3.2 ± 1.0	145 ± 12	0.3 ± 0.1*	9
AHF with DOB	3.5 ± 0.9	4.3 ± 1.4	56 ± 17†	7.4 ± 1.3	117 ± 6†	2.8 ± 0.8	156 ± 26†	0.6 ± 0.1	9
Loading run									
Baseline	2.9 ± 0.7	9.3 ± 3.2	24 ± 7	10.6 ± 4.5	161 ± 21	5.2 ± 2.4	127 ± 19	1.1 ± 0.7	7
NE	2.8 ± 0.6	10.9 ± 3.9	29 ± 9	14.8 ± 7.9†	165 ± 25	9.0 ± 5.4†	103 ± 24†	0.9 ± 0.4	7
SNP	3.1 ± 0.6	9.5 ± 3.6	19 ± 6*	9.1 ± 4.3	158 ± 31	4.6 ± 2.0	127 ± 17	1.3 ± 0.8	7
DEX	3.1 ± 0.9	7.2 ± 1.6	39 ± 10†	7.1 ± 3.5*	209 ± 26†	3.9 ± 1.9	107 ± 14*	1.2 ± 0.5	7
Heart rate run									
Baseline	2.8 ± 0.7	9.9 ± 3.0	24 ± 7	10.5 ± 5.0	155 ± 16	4.8 ± 2.3	134 ± 8	1.1 ± 0.7	6
ZAT	2.9 ± 1.1	6.9 ± 1.0*	39 ± 9†	6.6 ± 3.0	204 ± 33†	4.5 ± 2.2	86 ± 4†	1.2 ± 0.4	6
PACE	3.0 ± 1.4	10.0 ± 2.7	22 ± 9	18.4 ± 19.9	143 ± 22	6.9 ± 7.3	165 ± 12†	0.9 ± 0.4	6

Data are shown as mean ± SD (range). Because there was an overlap in baseline parameters between the loading and heart rate runs, the sum of the numbers of all interventions was not 82, but 76.

AHF, Acute heart failure induced by coronary embolization; *DEX*, dextran infusion; *DOB*, dobutamine infusion; *NE*, norepinephrine infusion; *PACE*, atrial tachypacing; *SNP*, sodium nitroprusside infusion; *ZAT*, zatebradine infusion.

*$P < .05$.

†$P < .01$ versus baseline.

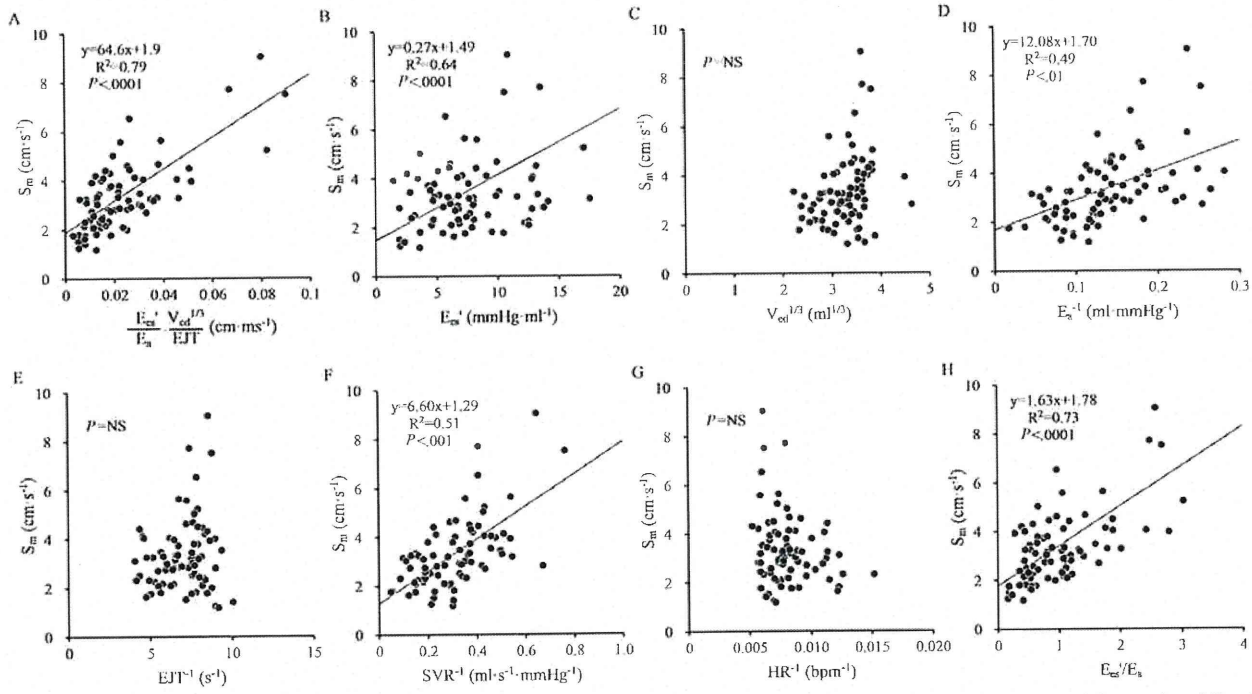

Figure 4 **(A)** Relationship between measured S_m and values obtained from the theoretical model consisting of the ratio of P_{es} to V_{es} (E_{es}'), V_{ed}, E_a, and EJT (see equation 1). **(B–H)** Relationships between S_m and E_{es}' **(B)**, the cubic root of V_{ed} **(C)**, the reciprocal of E_a **(D)**, the reciprocal of EJT **(E)**, the reciprocal of SVR **(F)**, the reciprocal of HR **(G)**, and the ventricular-arterial coupling ratio (E_{es}'/E_a) **(H)**. Each panel shows raw data from all interventions (76 data points) and the line representing the population-averaged regression between S_m and the cardiovascular parameters,[20] regression equation, R^2, and probability value.

phase, LV longitudinal and short-axis lengths change without change in LVV.[19] However, during the ejection phase, which was the phase of interest in our analysis, both LV longitudinal and short-axis lengths decreased in parallel with LVV. We also assumed that the ratio of LV longitudinal length to short-axis length is constant during the ejection phase (Appendix). The ratio is actually not constant. The ratio